TÉCNICO LISBOA

Study of the water dynamics into the CPVT system pipes

Michele Andreoli

Thesis to obtain the Master of Science Degree in

Energy Engineering and Management

Supervisors: Prof. Carlos Alberto Ferreira Fernandes

Prof. João Paulo Neto Torres

Examination Committee

Chairperson: Prof. Luís Filipe Moreira Mendes

Supervisor: Prof. João Paulo Neto Torres

Member of the Committee: Prof. João Filipe Pereira Fernandes

November 2017

RESUMO

Com o crescente interesse pelas energias renováveis, devido ao aumento de desempenho e à crescente necessidade de soluções mais sustentáveis para dar energia às nossas sociedades, os estudos sobre este tema têm-se tornado cada vez mais relevantes ao longo do tempo. Além disso, o desenvolvimento de programas de simulação virtual está a tornar-se mais fiável e, como resultado, fornece ferramentas novas e melhores para projetar e melhorar produtos e sistemas. A presente tese utiliza as tecnologias actualmente disponíveis para melhorar um coletor concentrado fotovoltaico-térmico (CPVT) produzido pela empresa Solarus AB. Após uma introdução das tecnologias utilizadas e uma descrição dos fenómenos físicos envolvidos no sistema, este trabalho estuda os efeitos térmicos e a distribuição de temperatura no receptor através do desenvolvimento de um modelo de simulação. O modelo desenvolvido analisa a mecânica dos fluxos de fluidos e a transferência de calor visando a optimização da temperatura nas células fotovoltaicas e na condução da água. Finalmente, o estudo apresenta análises dependentes do tempo; para perceber se as condições estacionárias já ocorrem durante o funcionamento normal do sistema e criar bases para novos trabalhos futuros, como a análise de aparas e problemas de fluxos de fluidos.

Palavras-chave: coletor fotovoltaico-térmico concentrado, análise de elementos finitos, energia renovável, otimização de eficiência.

ABSTRACT

With the rising interest in the renewable energies, due to the rise in performances and the increasing need for more sustainable solution to power our societies, the studies on the topic have becomes more and more relevant with the passing of time. In addition to this the development of the virtual simulation programs are becoming more reliable and therefore are giving new and better tools to design and improve the products and systems. This thesis uses the technologies available at the moment to improve a concentrated photovoltaic-thermal (CPVT) collector produced by the company Solarus AB. After an introduction of the technologies used and a description of the physical phenomena that are involved in the system; this work studies the thermal effects and the temperature distribution in the receiver through the development of a simulation model. The model developed analyses the fluid flow mechanics and the heat transfer aiming to the optimization of the temperature in the PV cells and in the water conduct. Finally the study introduces time-dependent studies; to understand if the stationary conditions ever occurs during the normal functioning of the system and to give the basis for new future works like the analysis of shavings and fluid flow problems.

Keywords: Concentrated photovoltaic-thermal collector, finite element analysis, Renewable Energy, efficiency optimization.

Index

Table index

Abbreviation list

Abbreviation	Description
3D	Three dimensional
CPVT	Concentrated Photovoltaic-Thermal
GGE	Greenhouse Gas Emissions
HCPVT	High Concentration Photovoltaic-Thermal
LCPVT	Low Concentration Photovoltaic-Thermal
MaReCo	Maximum Reflector Concentration
NOCT	Normal temperature of functioning of the photovoltaic cell
PV	Photovoltaic
CPV	Concentrated photovoltaic
PVT	Photovoltaic-Thermal
RES	Renewable energy source
STC	Standard test condition

Parameter list

Abbreviation	Description	Unit
A_{abs}	Absortion area	[m^2]
A_{ap}	Aperture area	[m^2]
A_{pan}	Area of the panel	[m^2]
A_{rec}	Receiver area	[m^2]
b	Temperature coefficient	[K^{-1}]
CF_{solar}	Solar Concentation Factor	[-]
C_p	Specific heat at constant pressure	[J/kgK]
D	Strain rate tensor	[m^3/]
Di	Internal diameter	[m]
D_o	Outside diameter	[m]
E	Internal Energy	[J]
E_{fluid}	Energy absorbed by the fluid	[J]
E_{in}	Energy in	[]J]
F	Volume force vector	[N/m^3]
F’	Collector efficiency factor	[-]
FF	Fill factor	[-]
g	Gravity acceleration	[m/s^2]
G	Irradiance	[W/m^2]
G^r	Reference irradiace	[W/m^2]
G_{abs}	Irradiance absorbed	[W/m^2]
GaSb	Gallium Antimonide	[-]
h	Convection heat transfer coefficient	[$W/(m^2K)$]
h_{fi}	Convection heat transfer coefficient inside the tube	[$W/(m^2K)$]
H_i	Irradiation	[kWh/m^2]
I	Identity matrix	[-]
I	Current	[A]
I_D	Diode current	[A]
I_{mp}	Maximum power current	[A]
I_{mp}^r	Maximum power current of reference	[A]
I_{PV}	Current created by the sunlight	[A]
I_S	Reverse saturation current	[A]
I_S^r	Reverse saturation current of reference	[A]
I_{sc}	Short circuit current	[A]
I_{sc}^r	Short circuit current of reference	[A]
k	Thermal conductivity	[W/mK]
K_B	Boltzmann constant	[J/K]
L	Characteristic lenght	[m]
m	Diode ideality factor	[-]
$\dot{m}$	Mass flow	[kg/s]
N_s	Number of cells in series	[-]
Nu	Nusselt number	[-]
p	Pressure	[Pa]
P	Power	[W]
P_{max}	Maximum power	[W]
Pr	Prandtl number	[-]
q	Charge of the electron	[C]
q	Heat flux	[W/m^2]
q_{cond}	Conduction heat flux	[W/m^2]
q_{conv}	Convection heat flux	[W/m^2]
q_r	Radiation heat flux	[W/m^2]

Q	Volumetric heat source	[W/m^3]
Q_p	Work done by pressure	[W/m^3]
Q_{ted}	Thermoelastic damping	[W/m^3]
Q_{vd}	Viscous dissipation	[W/m^3]
Ra	Rayleigh number	[-]
Re	Reynolds number	[-]
t	Time	[s]
T	Temperature	[K]
T_{amb}	Ambient temperature	[K]
T_{exp}	Experimental temperature	[K]
T_{ext}	External temperature	[K]
T_{in}	Inlet temperature	[K]
T_m	Temperature of the module	[K]
T_{out}	Outlet temperature	[K]
T_{ref}	Reference temperature	[K]
u	Velocity field	[m/s]
U	Bulk velocity	[m/s]
U_L	Energy loss coefficient	[$W/(m^2K)$]
V	Voltage	[V]
V_{mp}	Maximum power voltage	[V]
V_{mp}^r	Maximum power voltage of reference	[V]
V_{oc}	Open circuit voltage	[V]
V_T	Thermal voltage	[V]
α	Absorptivity	[-]
α_p	Coefficient thermal expansion	[K^{-1}]
ε	Emissivity	[-]
ε	Forbidden band	[eV]
η_{PV}	Electric efficiency	[-]
η_T	Thermal efficiency	[-]
μ	Dynamic viscosity	[Ns/m^2]
ρ	Density	[kg/m^3]
ρ_1	Reflectivity	[-]
σ	Cauchy stress tensor	[Pa]
σ_1	Stefan-Boltzmann constant	[$W/(m^2K^4)$]
τ	Viscous stress tensor	
τ_1	Trasmissivity	[-]

Figure Index

1 Introduction

Due to the increasing importance of the renewable energies, caused by the even more relevant negative impact that the human activities are having on the planet, the studies on the solar energy are gaining more and more importance to foster a development of a sustainable society. The scientific community is so concerned from these drawbacks of human development that there is an increasing consensus in the definition of a new geological era called the Anthropocene. In fact, the humans are the first species on the planet able with its behaviour to influence the rhythms of the world, producing a visible impact on the weather, on the biodiversity, on the landscape and many other aspects of the life of the planet. [1]

Solar energy is crucial in the development of a more environmental friendly future. Its importance as a renewable energy source (RES) is a consequence of several positive aspects of solar systems. In this context, it shall be highlighted that:

1. The sun´s radiation is converted into heat and electric energy; the heat is stored and is available for heating domestic water or building.
2. Solar system helps the reduction of greenhouse gas emissions (GGE).
3. Being dependent on the Sun, which is infinite when compared with the life of mankind, solar systems are almost inexhaustible.
4. Being an important alternative to fossil fuels, solar systems represent an important tool for energetic independence.
5. Solar systems are becoming more and more competitive in islands and rural areas where the energy cost is higher, reducing the costs of production and giving to these areas the opportunity to reach energetic independence.

With the increasing worldwide demand for energy, the solar energy is becoming more relevant for the production of thermal and electric energy.

The electric energy is produced through the photovoltaic (PV) effect, which transforms the power transmitted in form of solar radiation to direct current using semiconductors like silicon, which is at the moment the most used element, thanks to its low cost and higher efficiency when compared to other materials.

The photovoltaic effect is a physical phenomenon that can occur in the semiconductors when an adequate photon hits it, by the release of an electron-hole pair with the energy absorbed from the interaction. This effect is related to the conversion of radiative energy into electricity. This method of electrical energy production helps to reduce the carbon footprint, oppositely to the fossil fuel combustion. Pollution exists only during the creation of the photovoltaic cells and the construction of panels and associated installations.

The thermal energy is normally produced with the use of solar collectors that, when exposed to the solar radiation, transforms it into heat, warming air or liquids. These fluids flow by convection in the solar collector, once in there is heated by conduction, cooling the panel. Then the heated fluid reaches a tank

where it is stocked the fluid with a lower temperature. By convection the liquid continues to circulate in the solar collector, where it will be heated again.

The hybrid panels with concentrators, thermal and electric energy production, generally referred as C-PVT collectors, are systems used to produce both thermal and electric energy at the same time, increasing the amount of collected energy by the use of concentrator devices. Higher global efficiencies in the overall energy conversion are available and, consequently, the costs of production of the electricity are reduced. Moreover, the cooling effect introduced with the fluid circulation has a direct effect on the performance of the PV cells, which as will be shown in this study, is dependent on the working temperature. Finally, the increase in temperature caused by the solar radiation is partially recovered with the increase in the fluid temperature.

Solarus AB is a Swedish company, with the headquarters in the Nederlands and with a research centre in Gäyle in Sweden. The company is focused on the development of the thermal and hybrid (PVT) technologies. The panels developed by Solarus AB are characterized by an asymmetrical concentrator called MaReCo (Maximum-Reflector-Concentration). The hybrid panel analyzed in this thesis is formed by 2 receptor and 2 reflectors of equals dimensions, as shown in Fig.1. The design of the collector is studied to have a low solar concentration an to give the maximum solar radiation reflectance during all day without a tracking system.[2]

Figure 1 CPVT collector produced by Solarus AB[2]

1.1 Motivation

As previously referred, the increase in the demand for energy and the rising production of renewable energy are topics of increasing interest. Therefore, the improvement and the development of new

technologies are giving important opportunities to create a better future. These opportunities are sustained also by the economic competitiveness that the advancement will unlock.

The efficiency of the C-PVT panels depends on several factors, namely the reflection, the electric efficiency and, last but not least, the thermal efficiency. Many parameters can impoverish the collector performances such as a wrong solar incidence angle, a too high temperature, which harms the panels and the efficiency, a bad weather, which creates shadings, and an accumulation of dirt on the surface of the collector.

The main focuses of the research aim at to reduce the adverse effects in the collector, optimizing the temperature distribution and trying to develop a study method that could be used to study further the different problems; like those caused by the shadings and the uneven distribution of the temperature. Electric circuit configuration analysis will surely contribute to more convenient distributions of the electric and thermal energies in the collector. These two aspects, electric and thermal, are undoubtedly inter-related. The bi-directional electric-thermal interactions will be important and will certainly lead to complex questions/problems, due to the non-linearities involved. This thesis is mainly focused on the improvement on the thermal side of the collector, but it is expected to contribute to future analysis on the interactions between the two systems.

Objectives

The main focus of this thesis and the studies that it explain are the following:

- The study of the thermal effects that influence the design of a photovoltaic-thermal concentrator (C-PVT);
- The study of the temperature distribution in the receiver of photovoltaic-thermal collector, especially in the proximity of the photovoltaic cells and in the water conducts;
- The creation of a simulation model able to reproduce a fluid that flows in pipes in between the solar cells;
- The optimization of the temperature in the PV cells as a function of the ambient temperature and the solar irradiance;
- The study of the effect of a time-dependent phenomenon, in this case a variable irradiance, on the temperature distribution and on the efficiency of the photovoltaic part.

Thesis structure

This thesis is divided in 8 chapters that describe different main topic. The order of the chapters is the following:

- In chapter 1 is given a brief introduction to the main topic of the thesis describing the motivations behind it and the main purposes of this study;

- In chapter 2 is presented a summary of the state of the art explaining the different step of the development of the photovoltaic technology, of the thermal collector technology and of the hybrid technology (the PVT);
- In chapter 3 are shown the physical phenomena and the relative equations that regulate the behaviour of the receiver. In particular are explained the heat transfer phenomena, the fluid mechanics and the phenomena connected to the photovoltaic functioning;
- In chapter 4 are described the characteristics of the panel produced by the company Solarus AB and its specifics;
- In chapter 5 are presented the simulation in stationary conditions. In particular is compared the counterflow solution with the single direction solution that was already been studied in previous thesis;
- In chapter 6 are presented the simulations in time-dependent conditions. This approach represent an ulterior novelty because puts the base for a study with conditions similar to the operative ones and because it puts the base for the study of transitional phenomena like shadings;
- In chapter 8 are exposed the conclusions of the work and the suggestion for the future studies;

2 State of the art

2.1 Evolution of solar technologies

The use of solar energy to produce electricity is well known and its studies have been proceeding for more than a century. In fact, the first product capable of transforming the solar radiation into electricity, using the photoelectric effect discovered by Edmond Becquerel (1820-1891), is dated 1877 and had an efficiency of about 0.5%. From that moment to our days many things have changed and nowadays the efficiencies of the panels available in the market are close to the 22,5%, with some companies, such as Panasonic, that have already proclaimed they reached that levels, even though the panels are not yet available.[3][4][5][6]

Regarding the use of the energy that arrives from the Sun, as a source to produce heat, studies are even older: they were first started by the Swiss scientist Horace de Saussure in the year 1767. He performed an experiment in which, in order to heat water, he put the liquid inside a black painted box and then the box in another case made of glass and thermally insulated. With this method he managed to reach a temperature of 109 Celsius degrees (ºC) in the water. In the year 1908 the inventor William Bailey presented a patent in which was described a water heater quite similar to the solar collectors produced nowadays. For the first time the inventor was separating the storage from the heating part of the system. The separation of the two parts of the system reduced the heat losses during the night. In fact the storage was placed inside the house [7]. The modern solar collectors are able to reach levels of efficiency between 70 and 90%.

Due to the continuous development of the solar technologies, the use of the solar panel to produce only electricity was surpassed. In this way, it was introduced a new form of cogeneration in which the heat generation was added to the electricity production, creating the hybrid panels, both photovoltaic and thermal (PVT).

Unifying the thermal and the electric sides, the hybrid panels have to reach a compromise between the two technologies. In fact, it is quite impossible to maximise the two aspects at the same time and a different way to take the best gain from the Sun has to be found. With the adoption of this technology it is possible to obtain an improvement of the photovoltaic cells efficiency of about the 50%, since the increase of the temperature is a relevant limit to it. The big possibilities unlocked by the PVT technology are underlined from achievements like the reaching of the 44,5% efficiency, reached by the new PV panels that uses gallium antimonide (GaSb) substracts to absorb every part of the solar radiation [8]

The concentrated photovoltaic-thermal (C-PVT) panel presents three different possible configurations. The first one with a low concentration called LCPVT, which presents a concentration factor between 2 and 100 suns (the number of sun seen are a unit of measure of the concentrated light, where the number of suns means that the receiver is hitten by the irradiation that would see with the presence of that amount of sun in the sky). The second configuration are the medium concentration PV, that are those

that supports between 100 and 300 suns, requiring already two-axis solar tracking and cooling; therefore the complexity of the system is increased.The last configuration is with a high solar concentration and a concentration factor higher than 1000 suns (HCPVT). [9] The concentration factor, CF_{solar}, of the light presented above is obtained using the equation 1.

$$CF_{solar} = \frac{A_{ap}}{A_{rec}} \quad \text{(eq 1)}$$

Where A_{rec} is the area of the receiver and A_{ap} is the aperture area. [10]

2.2 Advantage and examples of CPVT

Higher efficiencies in CPVT technologies, when compared to thermal collectors and PV panels, justify their recent developments. The most important gains are:

1. A higher production of thermal an electric energy using the same technology;
2. A higher efficiency throughout the day thanks to the solar concentration that permits to reach peaks bigger than the 80%;
3. A higher power density (power per unit of area) that permit the reduction of the used area;[11]

Even if C-PVT collectors present the advantages described above, PVT and CPVT markets are still a small percentage of the photovoltaic and thermal totals. This is also a consequence of an inexistence certification or definition of quality to evaluate test and performances. This situation creates an obstacle to the adoption and the diffusion of the technology in the market. [10] [12]

To have a better comprehension of the technology behind the existing and underdevelopment CPVT collectors, five different cases will be described, namely: (*i*) concentrator with a parabolic trough, (*ii*) a concentrator with a cylindrical trough, (iii) a concentrator with asymmetric parabole trough and a (*iv*) concentrator with a parabolic dish.

Figure 2 Concentrator with parabolic trough [12]

Figure 2 above shows the parabolic trough with single axis tracking developed by the company SkyFuel. Due to the great heat reached in the centre of the concentrator, this system works with molten salt or thermal oil that creates fewer critical issues then water. [13]

Figure 3, shows a concentrator with a cylindrical trough and a single axis tracking system to improve the amount of energy harvested in a day. [14]

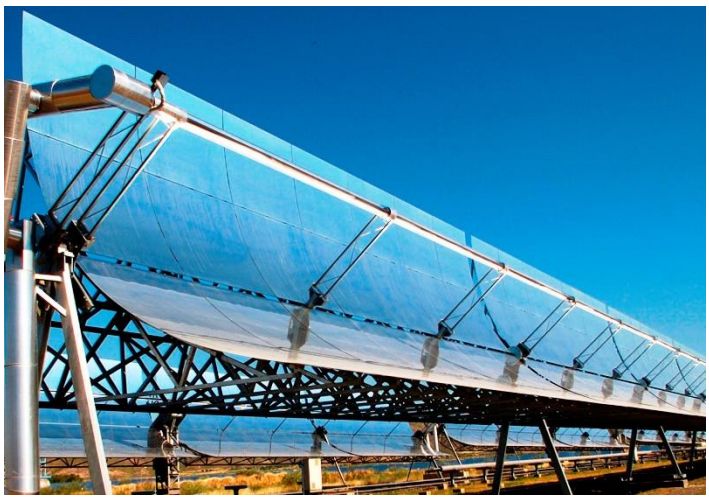

Figure 3 Concentrator with cylindrical trough collector

The next example of concentrated solar collector is an asymmetric parabolic trough built by Solarus AB presented in Figure 4. The asymmetrical shape and the receiver in the upper part give the advantage of avoiding the cost related to a tracking system.[2]

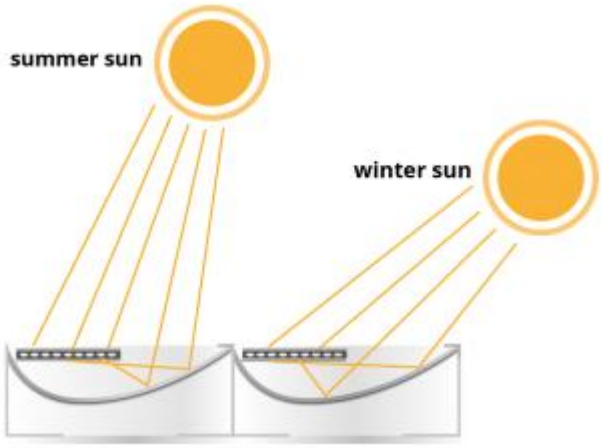

Figure 4 Concentrator with asymmetrical parabolic trough

The fourth case taken into account, in Figure 5, is a concentrator with a parabolic dish developed by Solartron energy system inc. The collector concentrates the radiation that hits a 63 m^2 area in a receiver

with dimensions 25x25 cm that sees the radiation equivalent of more than 1000 suns. The dish is also equipped with a two-axis tracking system that permits to increase the energy harvested during the day.[15]

Figure 5 Concentrator with parabolic dish[14]

The last example analyzed takes into account the more adopted form of concentrated PV, the Fresnel CPV that uses the lenses to concentrate the light of the Sun as shown in Figure 6. Concentrating the light, it becomes more possible to choose more expensive material due to the smaller area needed. This cells can in this way reach efficiency of 46% in the laboratory and give a module efficiency that can reach the 38,9%. [16]

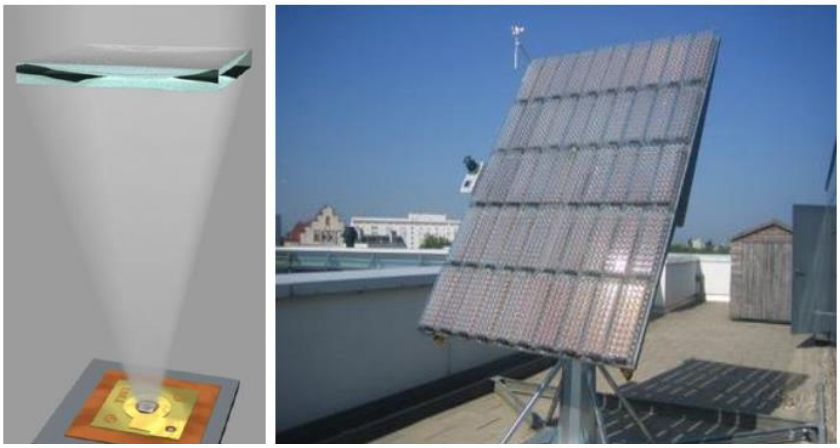

Figure 6 Example of a CPV using Fresnel lenses to concentrate the sun light. The working of the lense is presented in the left and the system is visible in the right. [16]

2.3 Solar radiation

To understand the effects of the solar radiation on the temperature of the studied technology, it is of crucial importance to understand the basics of the solar radiation. It is important to have some expertise on: (*i*) the different kinds of radiation; (*ii*) the different level of radiation distribution in the different areas, and (*iii*)the measurement of the power per unit of area received by the Sun.

2.3.1 Different kinds of solar radiation

The solar radiation that is emitted by the Sun in space toward Earth does not reach entirely the surface of the planet. In fact, the atmosphere acts like a shield and adsorb and deflect a part of the incoming beams. The remaining part of the radiation, that is able to surpass the atmosphere, can be divided into direct, diffused and reflected as shown in the Figure 7. The direct radiation is the component of the radiation that surpassed the atmosphere reach directly the examined surfaced. The reflected radiation is the part of the radiation that before reaching an object, in this case the receiver, hits other bodies and therefore loses a part of the initial energy. The remaining part of the radiation that reaches the receiver is called diffuse because it is diffused in the atmosphere or in the cloud before hitting the examined surface in an indirect way. The sum of the direct, diffused and reflected radiation is usually described as the global radiation.[17]

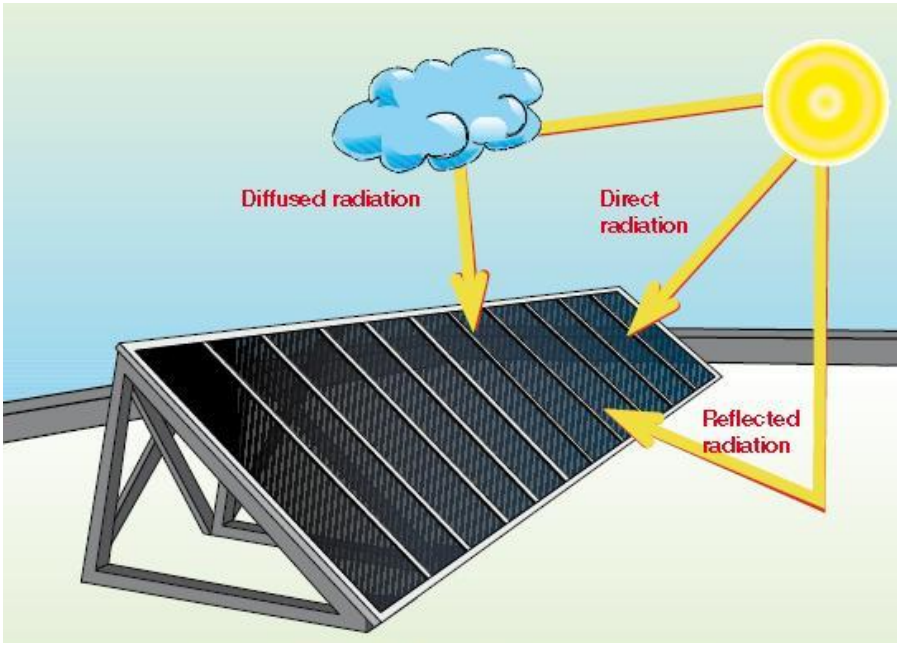

Figure 7 Components of the hitting radiation [15]

Figure 6 shows that often the surface is inclined, this happens in order to increase the radiation received during the day: This inclination is dependent on the latitude where the surface is installed and on the load curve that have to serve.

Solar irradiation (H_i), measured in kWh/m^2, is the solar energy per unit of area hitting the surface, while the solar power per unit of area is called irradiance, G, measured in W/m^2.

2.3.2 Temperature and irradiance in the different places

Since the solar radiation is one of the more critical parameters to evaluate the harvested energy, it is always necessary to analyse the local characteristics. In Figure 8 below it is shown the global solar irradiation in the world and underlined the differences in the different regions of the world. From the map we can also see how the irradiation does not depend only on the latitude.[18]

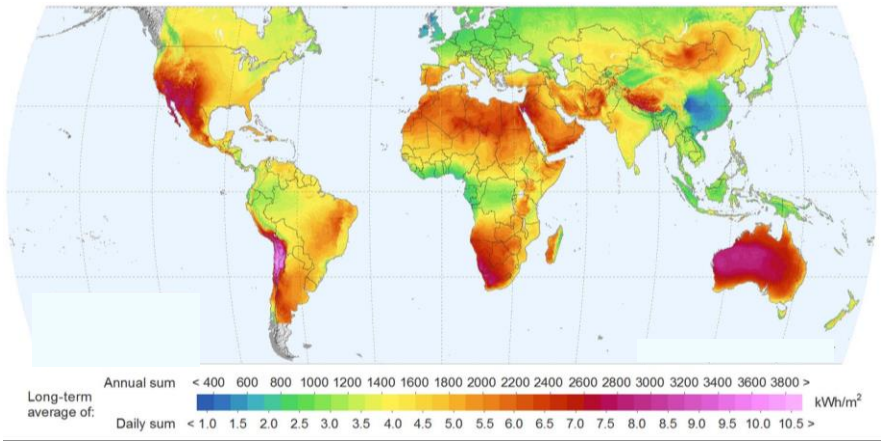

Figure 8 Irradiation in the world [kWh/m²] [16]

For the purposes of this thesis it is relevant the study of the influences of the temperature and of the solar radiation in winter (January) and in summer (July), for Lisbon and Gävle, on the performance of the CPVT collector. [19]

In Sweden during the winter, the average temperature can go below 0, in fact between 0 and -5 Celsius degree, and the solar radiation can oscillate between 0 and 150 W/m^2. On the other hand, in Portugal the temperature oscillates between 5 and 14 degree Celsius and the radiation can change between 0 and 600 W/m^2. This data are shown in the Figure 9 and in the Figure 10 below.

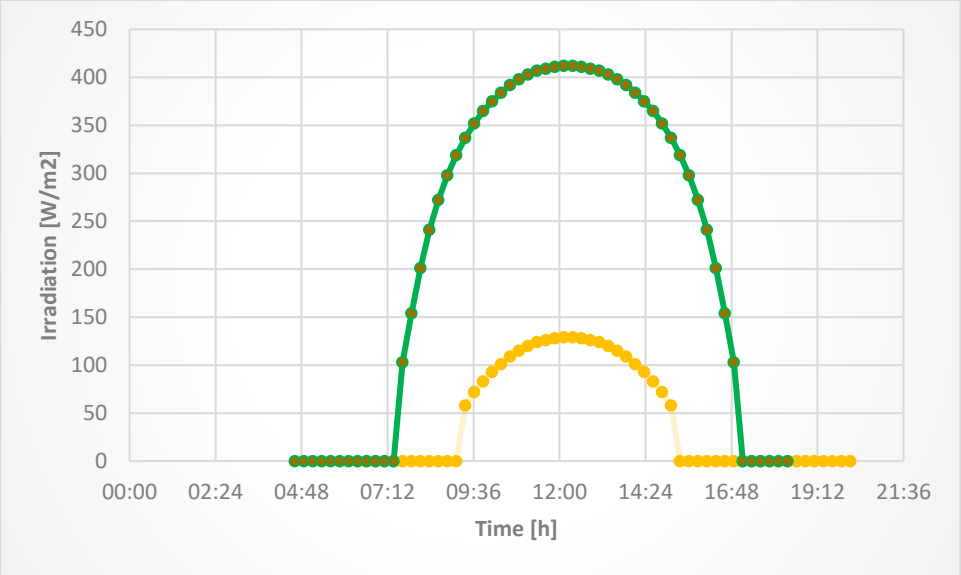

Figure 9 Irradiance during a winter day in Sweden (yellow) and in Portugal (green)

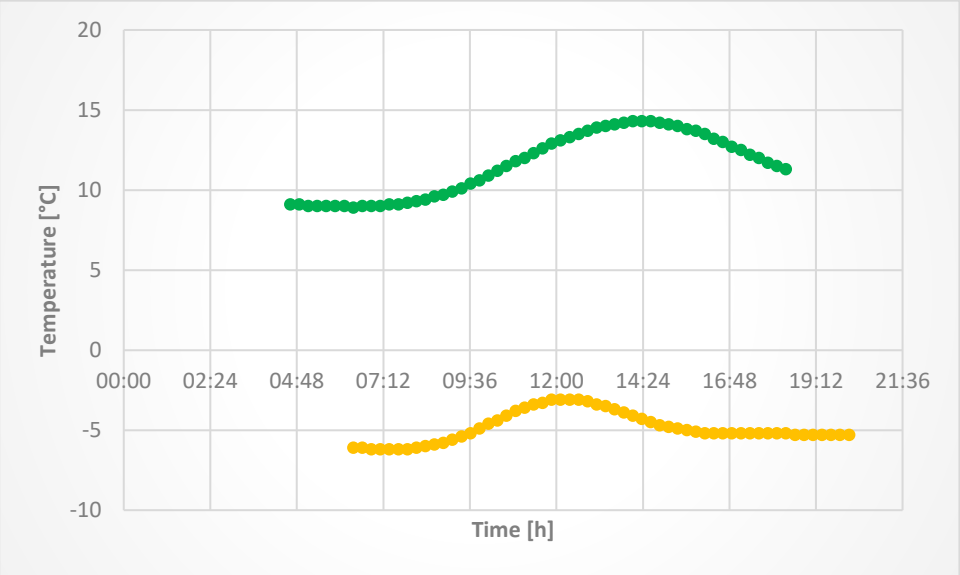

Figure 10 Temperature in a winter day in Sweden (yellow) and in Portugal (green)

In Sweden in summer, temperature reaches an average close to 20 °C, while the irradiance changes between 0 and 360 W/m^2. In Portugal, temperature values are between 17 and 28 °C and irradiance reaches 780 W/m^2. However, it is important to underline that due to the more hours of Sun hours in the Nordic country, the irradiances can be greater in Sweden in the sunrise and the sunset. The summer situation is shown in the Figure 11 and in Figure 12.

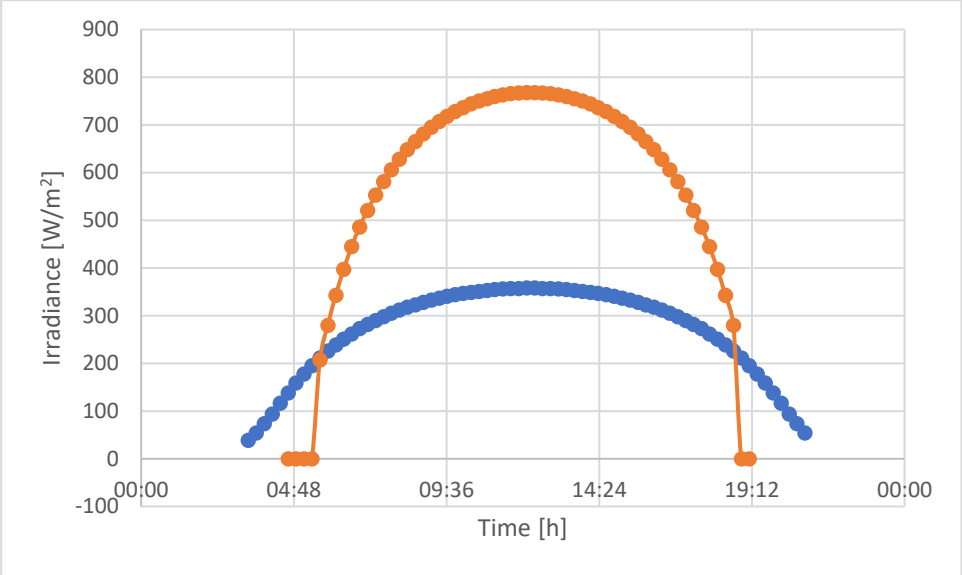

Figure 12 Irradiance in a summer day in Portugal (in orange) and in Sweden (in blue)

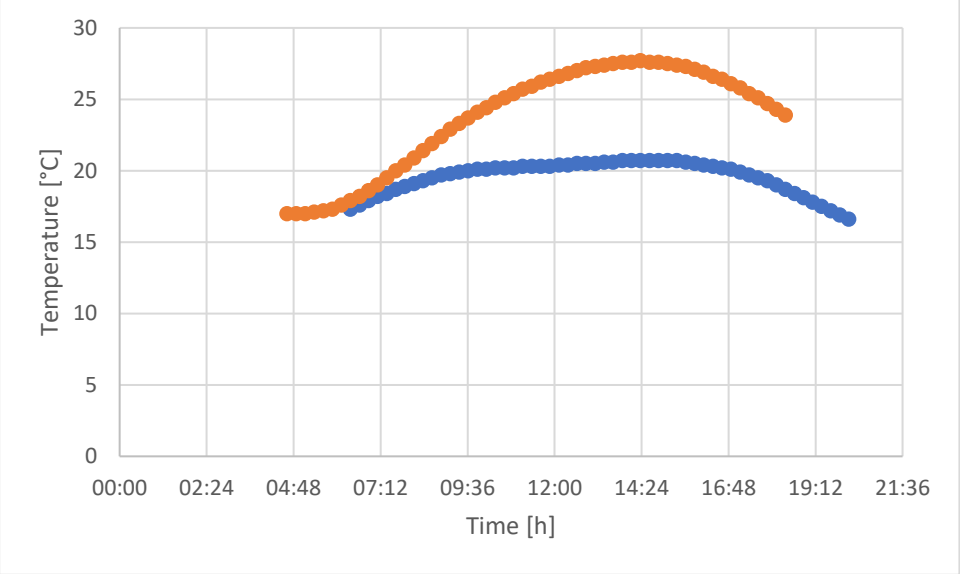

Figure 11 Temperature in a summer day in Portugal (in orange) and in Sweden (in blue)

Differences in irradiation and temperature along the year give the possibility of spending less in the cooling of the panels in places where the irradiation and temperature are lower. In fact the same mass flow of fluid will have more effect in a colder area than in a warmer place. It is then important to take into account the weather conditions to regulate the mass flow accordingly to the season.

3 Physical theory behind the collector

3.1 Heat transfer

To perform the study of the temperature in the CPVT it is necessary to understand the phenomena that govern the heat transfer.

Therefore, in order to describe the formulas that regulate this physical phenomenon we have to start from the analysis of the internal energy of a system that is not stable. In order to do that we will analyze the local heat balance equation in its spatial frame. The equation is reported below:

$$\rho \frac{\delta E}{\delta t} + \rho \boldsymbol{u} \cdot \nabla E + \nabla \cdot (\boldsymbol{q_{cond}} + \boldsymbol{q}_r) = -(\sigma : \boldsymbol{D}) + Q \qquad \text{(eq 2)}$$

Where ρ is the density, *E* is the internal energy, *t* is the time, *u* is the velocity field, q_{cond} is the heat flux by conduction, q_r is the heat flux by radiation, σ:*D* is an expression for the stress power where σ is the Cauchy stress tensor and D is the strain rate tensor, the term ":" is an operator (that can be written like a:b=$\sum_n \sum_m a_{nm} b_{nm}$) and *Q* is the additional volumetric heat source.

From equation (2), it is apparent how the time evolution of the internal energy (first element) must be equilibrated by the convection of the internal energy (second term), the heat flux through convection and radiation (third element), the losses due to the stress (fourth term) and the heat source (last element).[20]

3.2 Heat transfer in solids

The variation of internal energy of a solid is equal to the variation of temperature *T* multiplied by the specific heat capacity at constant pressure C_p. From Eq (2):

$$\rho C_p \frac{\delta T}{\delta t} + \rho C_p \boldsymbol{u} \cdot \nabla T + \nabla \cdot q = Q + Q_{ted} \qquad \text{(eq 3)}$$

In Eq (3) *q* is the total heat flux and Q_{ted} is the thermoelastic damping, a phenomenon that occurs out of thermal equilibrium when the structure starts vibrating.[21]

The second relation that we have to take into account for the heat transfer in solid is the Fourier's law for heat transfer. This one correlates the heat flux with the temperature using the thermal conductivity *k*. In its differential form is given by:

$$q = -k \nabla T \qquad \text{(eq 4)}$$

where $\vec{q}$ is the local heat flux density, expressed in [W.m^{-2}], *k* is the material's thermal conductivity, expressed in [W. m^{-1}K^{-1}], and ∇T is the temperature gradient, expressed in [K].[20]

3.3 Heat transfer in fluids

The formulas describing the situation in the fluids are slightly different because typical fluid physical interactions become relevant. In fact the thermoelastic damping disappears but two new terms become important: (*i*) the work done by pressure, Q_p, and (*ii*) the viscous dissipation, Q_{vd}. The new equation of heat transfer is given by:

$$\rho C_p \frac{\delta T}{\delta t} + \rho C_p \boldsymbol{u} \cdot \nabla T + \nabla \cdot q = Q + Q_p + Q_{vd} \quad \text{(eq 5)}$$

In (4) the viscous dissipation is described by the equation 6.

$$Q_{vd} = \tau : \nabla \boldsymbol{u} \quad \text{(eq 6)}$$

In (5) τ is the viscous stress tensor measured in Pa.
The work done by the pressure is expressed by the equation 7 that follows

$$Q_p = \alpha_p T(\frac{\delta p}{\delta t} + \boldsymbol{u} \cdot \nabla p) \quad \text{(eq 7)}$$

In (6) *p* is the pressure and α_p is the coefficient of thermal expansion described by:

$$\alpha_p = -\frac{1}{\rho}\frac{\delta \rho}{\delta T} \quad \text{(eq 8)}$$

Fourier's law, which describes the heat flux, is still valid.

3.3.1 Convective Heat Flux

To simulate a real heat transfer case is crucial to define how the heat is flowing from an element of the system to the other. There are three possibilities of flux convective, conductive and radiational.
The heat flux transferred by convection can generally be described by:

$$q_{conv} = h(T_{ext} - T) \quad \text{(eq 9)}$$

In the equation above it's clearly visible how the flux depends on the heat transfer coefficient, *h*, and on the difference between the external temperature, T_{ext}, and the one of the element analyzed, *T*. However, in many cases it is not easy to define the heat transfer coefficient, which is influenced by the geometry, the fluid material properties and the surface temperature.
To overcome this difficulty, we recur to formulas and relations which are normally based on many dimensionless numbers like the Nusselt number, Nu, the Reynolds number, Re, the Prandtl number, Pr, and the Rayleigh number, Ra, shown below.

$$Nu = \frac{hL}{k} \quad \text{(eq 10)}$$

$$Re = \frac{\rho U L}{\mu} \quad \text{(eq 11)}$$

$$Pr = \frac{\mu C_p}{k} \quad \text{(eq 12)}$$

$$Ra = \frac{\rho^2 g \alpha_p C_p \Delta T L^3}{\mu k} \quad \text{(eq 13)}$$

where *L* is the characteristic length, *k* is the thermal conductivity, *U* is the bulk velocity, μ is the dynamic viscosity, *g* is the acceleration of gravity and Δ*T* is the difference between the surface temperature and the external fluid bulk.
In order to simplify the exposition here will be exposed only the 2 cases used in this thesis.

3.3.1.1 INTERNAL NATURAL CONVECTION IN A CIRCULAR TUBE

In the case of natural convection in a circular tube the heat transfer coefficient can be expressed by the equation:

$$h = \frac{k}{H}\frac{1}{128}Ra \quad \text{(eq 14)}$$

Valid if *Ra* < H / *D*, where *H* is the length of the tube.

3.3.1.2 EXTERNAL NATURAL CONVECTION IN A LONG HORIZONTAL CYLINDER

When the natural convection takes place in a horizontal cylinder the heat transfer coefficient becomes

$$h = \frac{k}{D}\left(0{,}6 + \frac{0{,}387Ra^{\frac{1}{6}}}{\left(1+\left(\frac{0{,}559}{Pr}\right)^{\frac{9}{16}}\right)^{\frac{4}{9}}}\right)^2 \quad \text{(eq 15)}$$

3.3.2 Heat flux by thermal radiation

The second way that bodies may transfer heat is through thermal radiation. In fact, the bodies are normally emitting electromagnetic radiation and the amount of radiation emitted is a function of the temperature of the object. The exchange of heat by thermal radiation is regulated by the equation 16 below.

$$\alpha + \rho_1 + \tau_1 = 1 \quad \text{(eq 16)}$$

In which α is the absorption component, ρ_1 is the reflection component and τ_1 is the trasmission component. The absorption coefficient α is also equal to the emissivity**,** ε, which is the effectiveness in emitting thermal radiation. The radiative heat flux, simplified for a body surreounded by gray bodies, is described by the equation 17.

$$q = \varepsilon\sigma_1(T_2^4 - T^4) \quad \text{(eq 17)}$$

In the above equation σ_1 is the Stefan-Boltzmann constant (5.670367×10^{-8} W/(m^2·K^4)) and T_2 and T are the temperatures of the two objects. If the exchange of heat is with the environment, T_2 is equal to the ambient temperature, T_{amb}.[20]

3.4 Thermal efficiency

In the traditional thermal panels in order to evaluate the performance of the different types of collector the energy given to the fluid is measured and is put in relation with the energy received from the irradiance. This relation form the thermal efficiency of the fluid, η_T, defined in the following formula.

$$\eta_T = \frac{P_{fluid}}{P_{in}} \quad \text{(eq 18)}$$

The energy that is entering into the panel, P_{in}, can be described with the Equation 19.

$$P_{in} = G \times A_{abs} \quad \text{(eq 19)}$$

In which A_{abs} is the absorption area.

The power acquired by the fluid is defined in the next equation.

$$P_{fluid} = \dot{m} C_p (T_{out} - T_{in}) \quad \text{(eq 20)}$$

In the previous definition ṁ is the mass flow in kg/s, C_p is the heat capacity at constant pressure in J/(kgK), T_{out} is the temperature of the fluid at the exit and T_{in} is the temperature of the fluid at the entrance both measured in K. Normally the energy is transferred to the fluid with fluid channels that are normally, in a vacuum pipe, in parallel pipes, in pipes at serpentine or with other geometries of the pipes.

When the temperature of the panel is too low, close to the reference temperature (T_{ref}), the energy that the receiver manages to transfer to the fluid is lower and the thermal efficiency is lower. Therefore, in order to improve the performances is better to introduce a fluid with a temperature similar to the ambient temperature, as it will be shown in the following lines. The improvement in the thermal efficiency has also a positive consequence on the electric efficiency that benefits from the lower temperature of the better-refrigerated cells.

To consider the performances of the pipes in the removal of the heat a second way of expressing the thermal efficiency is defined.

In the second form of the thermal efficiency is introduced a new factor the collector efficiency factor of the PVT, F'. The efficiency factor can be defined with the Equation 21.

$$F' = \frac{\frac{1}{U_L}}{\frac{1}{U_L} + \frac{D_o}{h_{fi} D_i} + \left(\frac{D_o}{2k} ln \frac{D_o}{D_i}\right)} \quad \text{(eq 21)}$$

Where D_o and D_i represent the tube diameter respectively outside and inside, U_L is the energy loss coefficient measured in W/(m^{2}K) and h_{fi} is the convective heat transfer coefficient inside the tube.

With the defined efficiency factor defined and introducing also the correction coefficient (τα) in which τ represents the transmissivity and α represents is the absorptivity.

$$\eta_T = F' \times (\tau\alpha) - F' \times U_L \left(\frac{T_m - T_{amb}}{G}\right) \quad \text{(eq 22)}$$

In which T_m is the medium temperature of the fluid, that is the average of the temperature of inlet and the temperature of outlet.

Using the thermal efficiency in his formula shown above is possible to obtain the relationship between the thermal efficiency and the difference of temperature between the experimental one and the ambient one, this relation is shown in the figure 13 below.

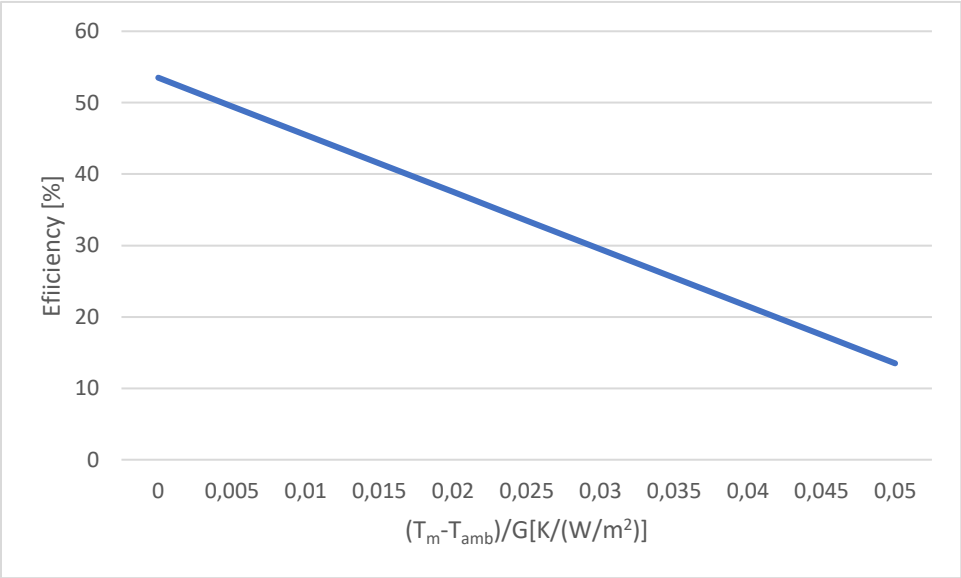

Figure 13 Thermal efficiency as function of difference of temperature and irradiance

In the picture above can be seen that the thermal efficiency is inversely proportional to the difference in temperature between the experimental temperature and the ambient temperature. However the thermal efficiency does not depend only on the difference of temperature and the irradiance but also on the thermal insulation, the speed of the wind, the material of the absorbing surface and others. [22]

3.5 Fluid flow theory

Basically, the fluid flow theory governs the forces of attraction between the molecules of fluids. The motion of fluid viscous substances is governed by the Navier-Stokes equations. These are the continuity equation, that represents the conservation of mass, and the equation that describes the conservation of momentum. The former is given by:

$$\frac{\delta\rho}{\delta t} + \nabla \cdot (\rho \boldsymbol{u}) = 0 \quad \text{(eq 23)}$$

Where ρ is the density, expressed in [kg·m^{-3}], and $\boldsymbol{u}$ is the flow velocity, expressed in [m/s].

Conservation of momentum is given by:

$$\rho \frac{\delta \boldsymbol{u}}{\delta t} + \rho(\boldsymbol{u} \cdot \nabla)\boldsymbol{u} = \nabla \cdot [-p\mathrm{I} + \tau] + F \qquad \text{(eq 24)}$$

where I is the identity matrix, *p* is the pressure, τ is the stress tensor and *F* is the volume force vector (in N/m^3).

In incompressible flows the density remains almost constant. In those cases the Navier-Stokes equations may be simplified, and equations (23) and (24) may be replaced, respectively, by:

$$\rho \nabla \cdot \boldsymbol{u} = 0 \qquad \text{(eq 25)}$$

$$\rho \frac{\delta \boldsymbol{u}}{\delta t} + \rho(\boldsymbol{u} \cdot \nabla)\boldsymbol{u} = \nabla \cdot [-pI + \mu(\nabla \boldsymbol{u} + (\nabla \boldsymbol{u})^T)] + F \text{(eq 26)}$$

In (26) μ is the dynamic viscosity, expressed in [Pa·s].[23] [24] [20]

3.6 Simplified electric model

In order to describe the functioning of the CPVT collector is essential to understand the phenomena that govern the photovoltaic cells.

The photovoltaic cells are often represented with the equivalent electric circuit that describes the functioning of the PV cell as if it was a traditional circuit composed by traditional elements. The simplified version of this circuit, which is normally used, is shown in the Figure 14 below. In particular the cell is substituted with two elements a current source, that depends on the light that reaches the cell, representing the electricity generated and a diode in parallel describing a conventional junction. [25][26]

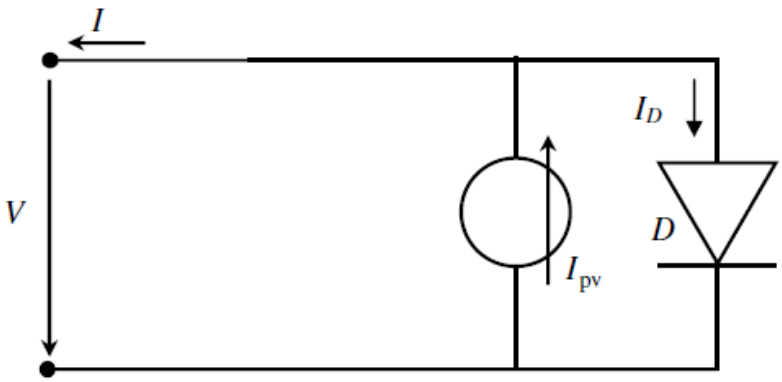

Figure 14 Simplified electric circuit

In the Figure 14, I_{pv} describes the current created by the solar light, I_D is the current lost in the diode, D is the diode, I is the current that goes out from the PV cell and V is the terminal voltage. The current that comes from the cells, I, can be described with the equation 27 below.

$$I = I_{pv} - I_D = I_{pv} - I_S(e^{\frac{qV}{mK_BT}} - 1) \qquad \text{(eq 27)}$$

Where I_S is the reverse bias saturation current, q is the module of the charge of the electron, m is the diode ideality factor, K_B is the Boltzmann constant and T is the absolute temperature. Often in this formula is also introduced the thermal voltage defined by the equation 28.[26]

$$V_T = \frac{K_B T}{q} \qquad \text{(eq 28)}$$

3.6.1 Working point of the PV cells

During the functioning of the solar cell the values of I and V are positive following the direction is shown in the Figure 13 above. The electric model of the panels depends on the connections, in series or in parallel, between the cells that form the panels and can change from panel to panel. The key parameters that describe the panels specifics paper are always calculated in standard test condition, STC, that are an ambient temperature of 25 °C and an irradiance of 1000 W/m^2.

The key parameters are two voltages and two currents. The two voltages are the are the open circuit one, V_{oc}, and the maximum voltage, V_{mp}, the first one corresponds to no load and is the maximum tension generated by the panel, the second one is the voltage measured at the working point when is at the peak of the power.[26]

The two currents are the short circuit current, I_{sc}, obtained when the voltage is zero and therefore is the maximum obtainable current, and the maximum power current, I_{mp}, that is the current at the working point when the power is at its maximum. In the next image, Figure 15, is visible the current as a function of the voltage in blue and the power as a function of the voltage in orange.

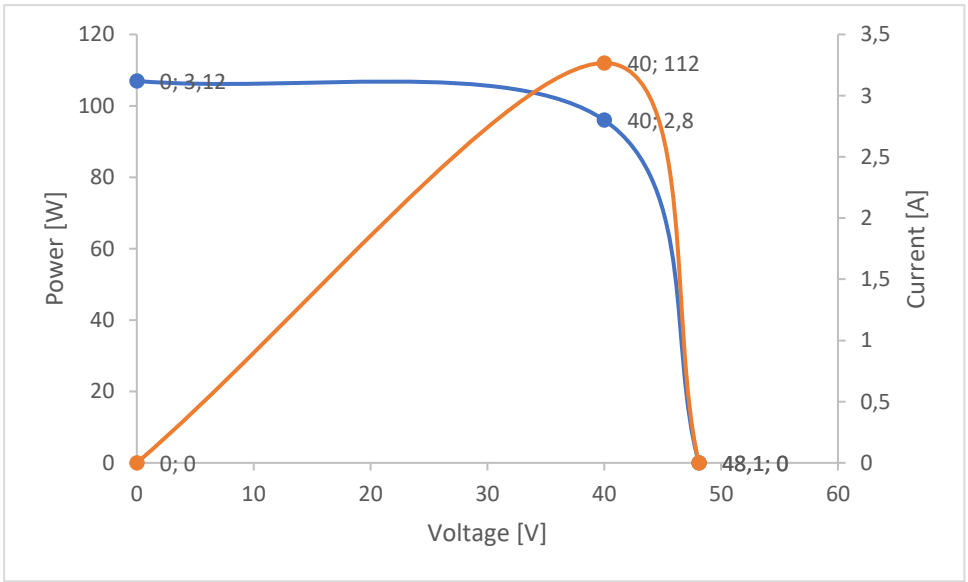

Figure 15 I-V curve for a solar panel (in blue) and P-V curve for a solar panel (in orange)

One of the most important parameter to evaluate the performances of the panels is the Fill Factor, FF, defined in the equation 29 that follows.

$$FF = \frac{P_{max}}{V_{oc} \times I_{sc}} = \frac{V_{mp} \times I_{mp}}{V_{oc} \times I_{sc}} \quad \text{(eq 29)}$$

In which P_{max} is the maximum power. The Fill Factor represents the ratio between two areas, the one given by the product of $V_{mp} \times I_{mp}$ that represent the maximum power and the area given by $V_{oc} \times I_{sc}$ that is a non reachable power. Therefore the Fill Factor will be always lower than one by definition. The following image, Figure 16, shows the rappresentation of the two areas defining the Fill Factor where the yellow area is the maximum power.

Normally the Fill Factor of the panels is above 0,7. [25]

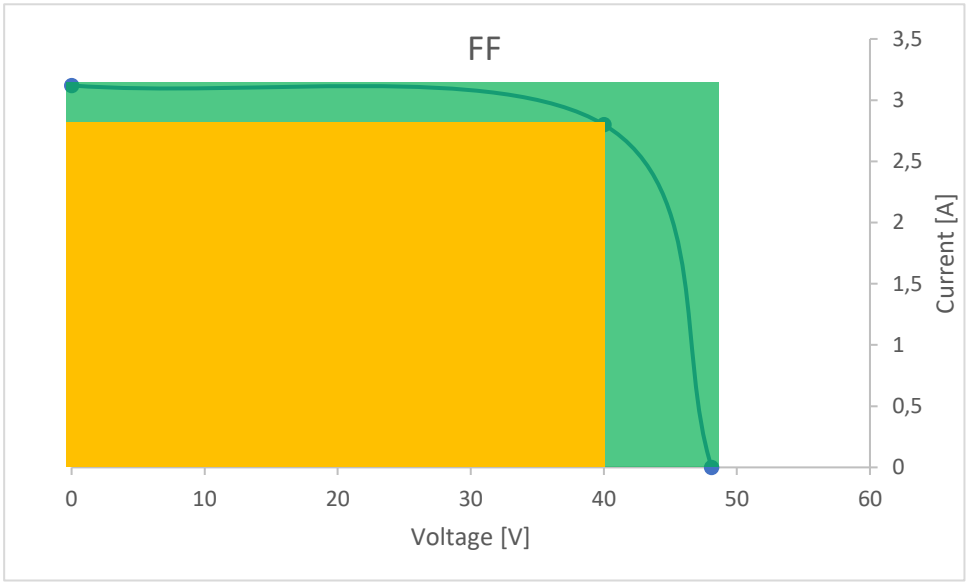

Figure 16 Fill Factor with the I-V curve

3.7 Electric efficiency

Another very important parameter to describe the characteristic of functioning of the panel is the electric efficiency, which can be negatively affected by the high temperature, by the shading or by the low radiation. The electric efficiency is defined with the equation 30 below.

$$\eta_{PV} = \frac{P}{G \times A_{pan}} \quad \text{(eq 30)}$$

In the formula above G is the Irradiance measured in W/m^2, P is the power produced by the panel in W and A_{pan} is the area of the panel. To define the peak power, P_P, the following equations that describe the voltage and the current at the maximum power point are used.

$$I_{mp} = I_{sc} - I_S(e^{\frac{V_{mp}}{mV_t}} - 1) \quad \text{(eq 31)}$$

$$V_{mp}^{k+1} = mV_t \ln\left(\frac{\frac{I_{sc}}{I_S}+1}{\frac{V_{mp}^r}{mV_t}+1}\right) \quad \text{(eq 32)}$$

$$I_{sc} = (\frac{G}{G^r})I_{sc}^r \quad \text{(eq 33)}$$

$$I_S = I_S^r \left(\frac{T_m}{T^r}\right)^3 e^{\left(\frac{\varepsilon N_S}{m}\left(\frac{1}{V_T^r}-\frac{1}{V_T}\right)\right)} \quad \text{(eq 34)}$$

Where m is the ideality factor, the terms with the r as an apex are the reference terms, ε is the energy of the forbidden band (that for the silicon is 1.12 eV) and N_s is the number of cells connected in series. The maximum power voltage is calculated with the equation 32 with an iteration method and then is used for the calculation of the maximum power current. Then with the previous equations the peak power is calculated. [27]

$$P_P = V_{mp}^r I_{mp}^r \quad \text{(eq 35)}$$

3.7.1 Dependence of the electric efficiency on the temperature

The production of electricity in a PV panel is due to the effect of the solar incident radiation in the pn junction present in the panel. The variation of temperature in the semiconductor has effects both the production of electrons and the internal resistance of the PV. However, even if the effect on the production of electrons is positive because are increased, the negative effect on the internal resistance make drop the efficiency of the panel. This is caused by the higher number of collisions that take place inside the material impeding the increase of electricity output and increasing even more the temperature. The effects of the temperature on the I-V curve are shown in the Figure 16 above, in which is visible that how the negative effect of the temperature on the voltage is bigger in magnitude than the positive effect on the current.

The consequences of the temperature effects are visible in the Figure 17 that shows the reduction of performances due to the high temperatures.

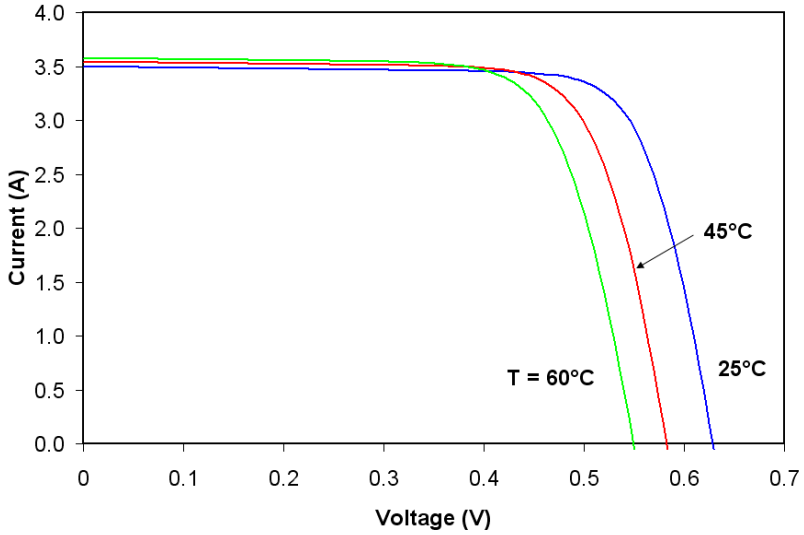

Figure 17 Effects of the temperature on the I-V curve

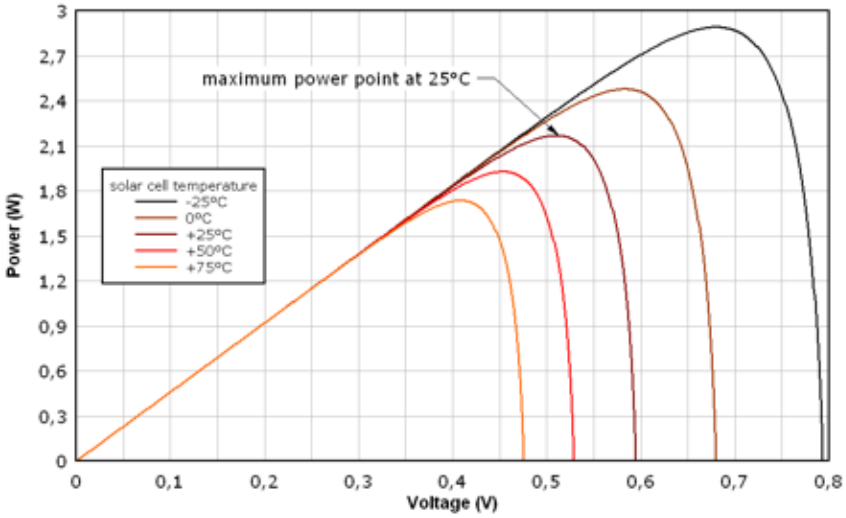

Figure 18 Variation in the P-V curve with the changing temperature [26]

From the Figure 18 it can be observed that the power produced decreases of about the 25% with an increase of temperature of about 50 degrees.[28] The reduction of the power output has naturally also an effect on the efficiency of the panel. The variation of efficiency caused by the temperature variation can be calculated using the equation 36 that follows

$$\eta_C = \eta_{ref} + b(T_c - T_{ref}) \qquad \text{(eq 36)}$$

Where the terms with the subscript c are valid at the analysed temperature, the terms with the subscript ref are those calculated at the reference temperature and b is the temperature coefficient that is a parameter typical of each panel. It is important to underline that the second addend is always negative when the temperature considered is higher than the reference one. [29]

3.8 Effects of irradiance

Among the different parameters that are affecting the output of energy from the panel certainly has relevance the irradiance, that as seen in the in the previous paragraph appears in the equation 33 and therefore influences also the equations 31, 32 and 34.

The Figures 19 and 20 that are following are showing respectively how the I-V curve and how the P-V curve are influenced by the irradiation. From these pictures is possible to notice how the decrease of the 20% of the irradiance has a linear effect on the reduction of produced current. However, due to an effect also on the voltage, even if smaller(smaller then the 10% with an irradiance variation of the 60%), the effect on the power produced is bigger, being around the 25% with the same 20% reduction. [28]

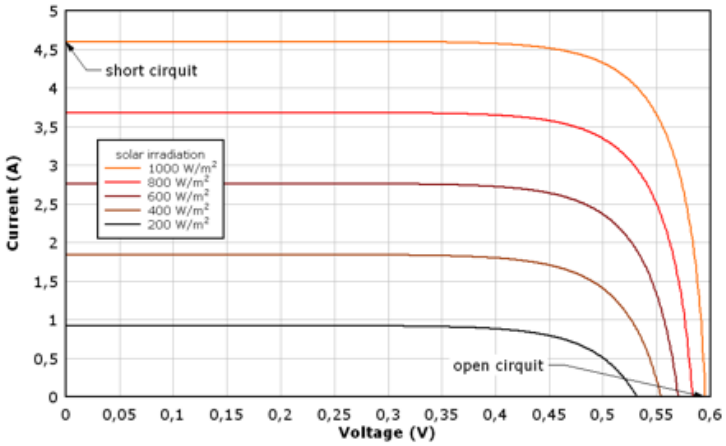

Figure 19 Variation of the I-V curve in function of the irradiance [28]

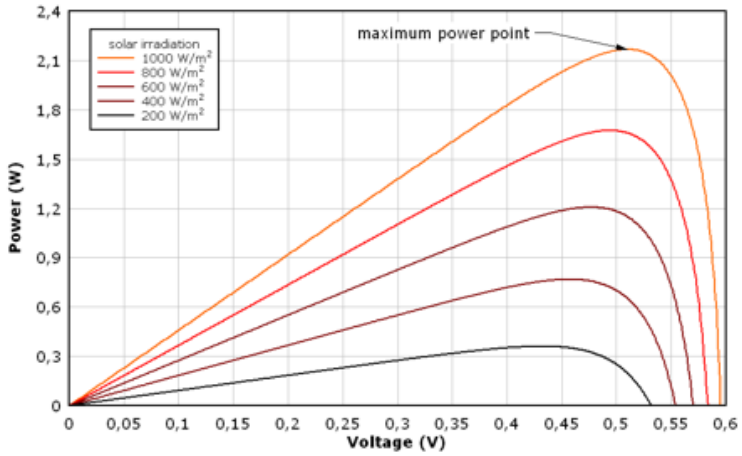

Figure 20 Power characteristics of the solar cell for different irradiance level [28]

The irradiation has also another important effect on the panel, in fact is one of the three variables that influence the temperature of the module, T_m, together with the ambient temperature, T_{amb}, and with the normal temperature of the functioning of the photovoltaic cell, NOCT. The formula that defines the module temperature is shown below.[30]

$$T_m = T_{amb} + \frac{G(NOCT-20)}{800} \qquad \text{(eq 37)}$$

The NOCT parameter is defined as the temperature that the cells reach with the open circuit at standardized conditions which are:

1. Incident irradiance of 800 W/m^2,
2. Ambient temperature of 20 °C,
3. Velocity of the wind of 1 m/s,

3.9 Shading in the photovoltaic cells

Before the installation of technologies with photovoltaic cells is always needed a study of the local characteristics, in fact the solar radiation is essential to produce energy. The parameters that influence the radiation need to be carefully analysed in order to maximise the production. In this regard the effects of the shadings are always considered due to their negative consequences on the energy output and on the life of the panels. The damages on the output and useful life are caused by the increase of internal resistance with a direct effect on the energy dissipated increasing the temperature of the cells. When the energy dissipated is too much the temperature can reach critical levels and the cells can be damaged. This damages can caused by the shadings when they affect one of the cells connected in series in a panel creating a bottleneck in the circuit. In order to avoid this bypass diodes are introduced in the circuit. [31][32]

The types of shadings are two: the total shading and the light shading.

When the shading is light the voltage is almost not affected, however the current production is reduced due to the smaller irradiance that hits the solar cells. This type of shading is produced when the atmospheric conditions are particular or when the clouds impede to a part of the radiation to reach the cells. This provokes a diminution in the incident power and therefore in the output of the panel.

The second type of shading, the total one, is caused by solids that project their shadows on the panels creating an obstacle in the light path. When a part of the cell is illuminated the current produced is proportional to the fraction of the cell that receives the light. The three different possibilities are shown in the image below, Figure 21.

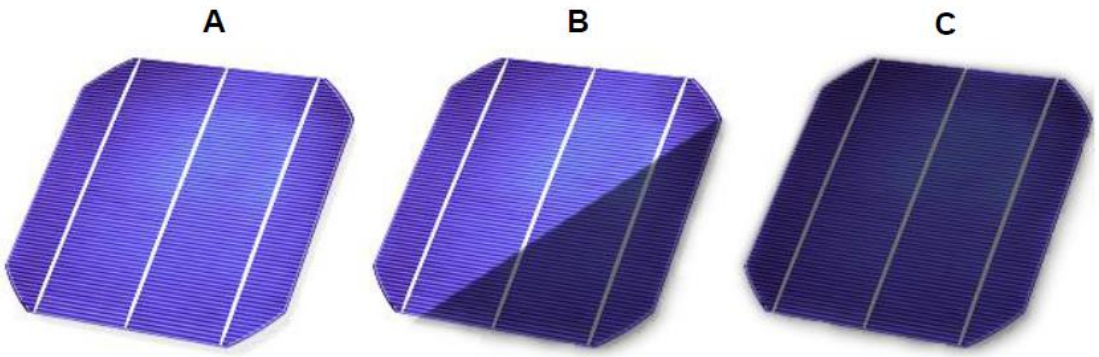

Figure 21 Different possibilities of shading: without shading (A), with partial shading (B), with total shading (C)

When the cell is completely illuminated, case A of the picture above, the cell work at full capacity. In the second case, the case B of the image, the shading is partial and as said before the current produced depends on the illuminated part. The last possibility, the case C of the Figure 21, the shading is total and the production is zero because the power received by radiation disappears. [33]

The negative effects of the shadings are even more relevant in the panels because of the cells connected in series. In fact, the energy produced by the cells is limited by the cell with the bigger shading that impedes the flow of the current coming from the more illuminated cells. Therefore the energy that is produced by the less shaded cells is dissipated in form of thermal energy that increases the negative effects on the efficiency.

In order to improve the performances of the solar panels and to reduce the negative effects of the shadings the manufacturers of the PV are introducing bypass diodes in parallel to the different series of cells to avoid losses in the shaded cells. In facts, the diodes give to the current a way to flow without passing in the series where the energy is lost. However, the introduction of these diodes increases the costs of production having higher number of elements in the panels. Therefore the different companies are always studying the best disposition and number of the diodes to reach the best compromise between performances and costs.[32]

4 Solarus panel

4.1 Panel geometry and characteristics

The geometry of the solar panel created by the company SOLARUS AB is formed by two PV panels applied on a aluminium block that has two main functions one structural and one related to the cooling of the photovoltaic panels, in order to increase their efficiency during the work. In fact in the metallic block are realized eight holes which have the function of conducting water across the block. The water flowing in the system permits to have two beneficial effects:

1. The reduction of the temperature at which the PVs are working, increasing their efficiency.
2. The production of extra energy, in form of heat.

The shape of the pipes is elliptical because, as described in the thesis realised by Pedro Alves [35], this shape permits to reach a compromise between the surface of exchange and the more uniform

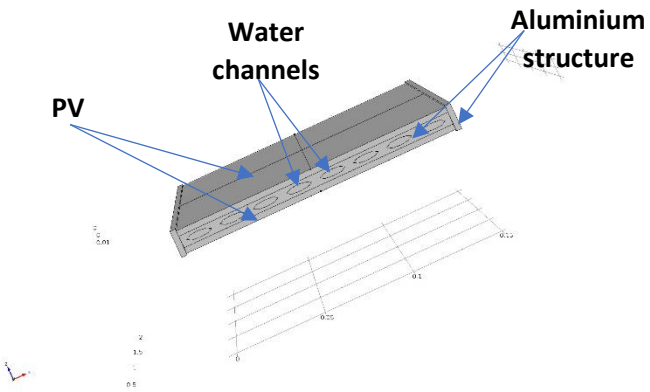

Figure 22 Geometry of the receiver structure

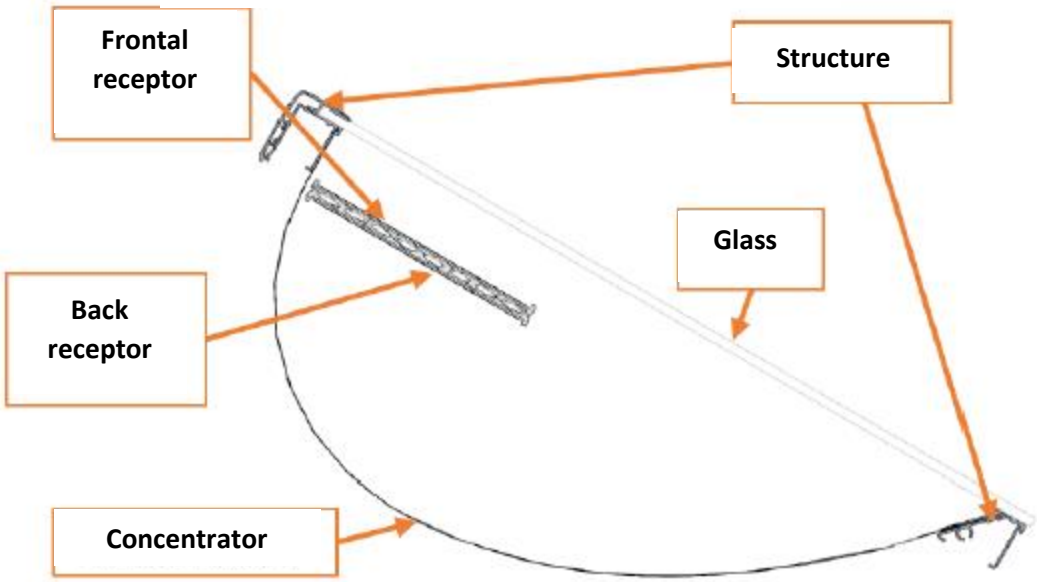

Figure 23 CPVT structure [35]

temperature of the fluid inside the pipe. The shape of the two PV on the aluminium structure is visible in the Figures 22 and 23.

The receiver is the most important element of a bigger structure the concentrating photovoltaic-thermal panel (CPVT). This type of system let enter into the structure more light than the one that hits the frontal PV. Then, thanks to a mirror placed behind the main panel structure, the system concentrate the light that is in the cavity and has not hitten the frontal PV on the one situated in the back. This approach permits a better usage of the space reducing the cost of the receptor, which is the higher, by exposing the PV in the back to a concentrated light (basically the PV reacts to a stronger irradiation as if more than a sun was hitting it). The structure is shown in the Figure 23 above.

The more detailed technical properties of the CPVT are shown in the tables 1, 2 and 3 below. The data were taken from a previous thesis [35] because the website of the company, that was also reported as a source in the previous work, is now changed and does not show the same information [2]. Moreover, the data reported are or slightly different or more approximated. Therefore, in order to use coherent data and to progress from the study already made the data from the previous study were used, supposing that the change in performance would have been small and positive (the panel cannot have worse performance than those already made).[2]

Table 1 General properties of the collector

Dimensions (L x W x H)	1027 x 2374 x 231 mm
Weight	55 Kg
Aperture area	2.2 m^2
Cover	4 mm anti-reflective coated glass, super transparent, hailstone safe

Table 2 Electrical properties

Cells number	152
Cells dimensions	52 x 148 x 0.2 mm
Peak electric power	250 W ±5%
Type of photovoltaic cells	Monocrystalline
Electric efficiency	18.9%
Temperature dependence	-0.43%/K

Table 3 Thermal properties of the collector

Heat loss coefficient	4.8 W/(m^2K)
Peak thermal power	1250 W
Capacity antifreeze	1.4 l/module
Maximum working pressure	6 bar
Maximum working temperature	175°C

4.2 Material composition of the receiver

The materials that are present in the receiver are shown in Figure 24 and are numbered according to the following enumeration:

1. Silicone;
2. PV cells (silicon);
3. Aluminium;
4. Water channels;
5. Electric conductor;

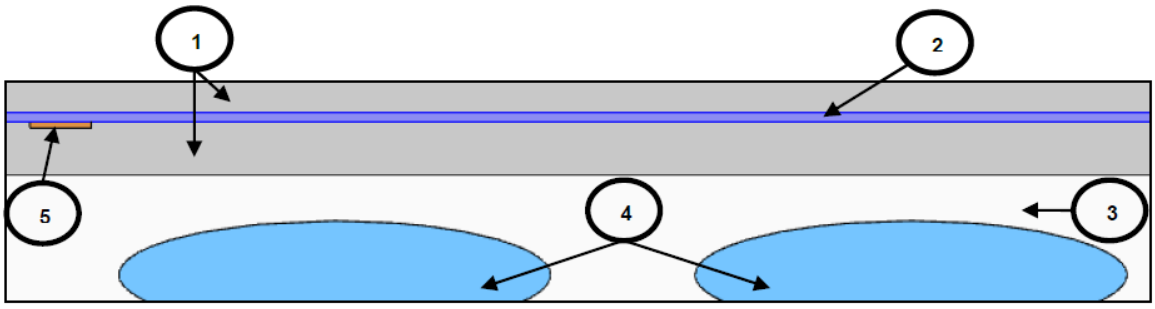

Figure 24 Representation of the five materials of the receiver

Every material has a clear function in the receiver. In order to obtain the best result in the energy output, the photovoltaic cells are made of monocrystalline silicon to produce the electricity with better efficiency.

The silicone has the principal functions of giving electric insulation to the cells, to avoid losses and short circuit, and of giving a high transmittance of the light permitting to have a maximized incident radiation.

The material that is presented in the biggest quantity is the aluminium that needs to facilitate the heat conduction between the silicone and the water channels that cools the panels.

The electric conductor is a piece of copper that creates the electric connections among the different photovoltaic cell.

The last components is the water that has the crucial function of cooling the photovoltaic cells and at the same time take advantage from the obtained heat using this thermal energy.

The more crucial parameters for the different materials are summarized in the Table 4 below. [35]

Table 4 properties of the materials used in the receiver

	Thickness [mm]	Thermal conductivity [W/(mK)]	Density [kg/m^3]	Heat capacity at constant pressure [J/(kgK)]
Silicone	2.7	0.2	970	1400
Photovoltaic cells (silicon)	0.3	148	2330	870
Aluminium	6.5	204	2700	870
Water	3.5	0.58	997	4187
Electric conductor (copper)	0.2	400	8700	385

5 3D Simulation of the panel in stationary conditions

5.1 Computational simulation of a physical problem

Special simulation tools are often used to study the performance of devices/products, reducing costs related to the prototyping and lab simulations. In this context, studies recurring to the finite element method has been used.

The finite elements method consists in a study of many smaller sub-systems that together create the complete object under study. Every sub-system is an element of the study and is associated with a partial differential equation, which is solved using mathematical methods. A more accurate and careful reproduction of the physical phenomena imposes an increase in the numbers of studied elements, and, therefore, an increase of the computation time. In this thesis, the digital simulation was conducted using three-dimensional elements shown in Figure 25.[34]

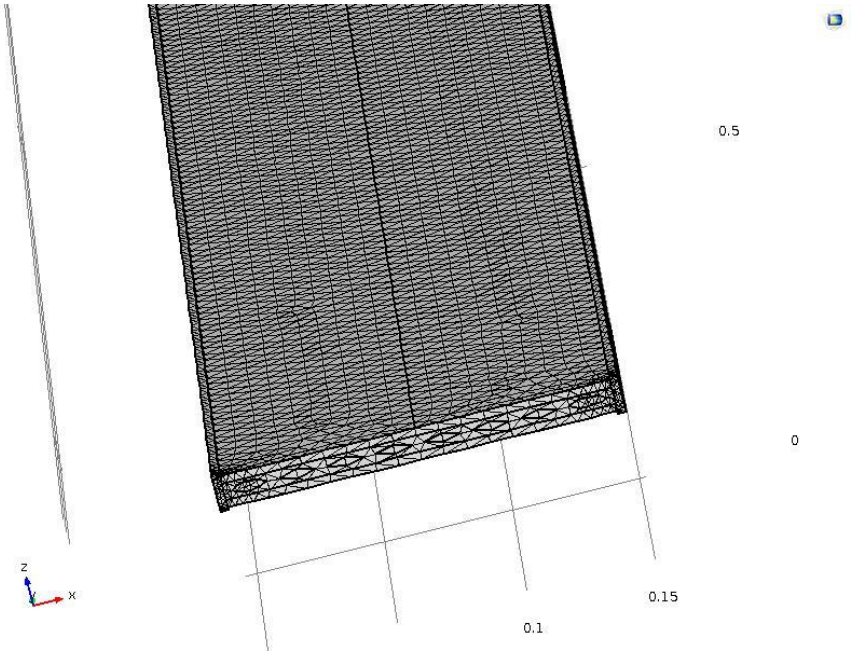

Figure 25 Image of the grid used to study the PVT panel

The simulations analyzed in this thesis as already said before are the developments of the work already done in a previous thesis, therefore was analyzed directly the problem in a three-dimensional approach. To have clear and consistent results and understand the simulation is necessary to define some constants. These constants can be dependant on the weather (wind, temperature, radiation from the sun) or can be physical properties (dimensions or characteristics of the different materials).

5.2 Initial conditions and fixed parameters of the simulation

As just said in the previous paragraph some parameter have to be fixed in order to measure and compare the different simulations obtaining valid conclusions. The two most important parameters that need to be defined are the convective heat transfer coefficient from the cells to the outside, $h_{conv,}$ and the velocity of the fluid in the conducts. The first parameter as explained in the previous parts of the thesis depends normally on many other characteristics, of the panel and physical, therefore to avoid complicated supposition and formulas the convective heat transfer coefficient is calculated using the following formula 38.

$$U_T = \frac{1}{\frac{1}{h_{conv}} + \frac{L_i}{k_i}} \qquad \text{(eq 38)}$$

In which U_T is the total heat loss coefficient, L_i is the length the heat has to pass through in the solid and k_i is the thermal conductivity of the material. Considering the length as the half of the silicone depth and obtaining the conductivity from the program we obtain an h_{conv} equal to 4.936326 W/(m^{2}K).

The velocity of the fluid depends on the volumetric flow that is imposed. To maintain the comparison with the previous study the flow is of 2 L/min per pipe. Using the Equation 39 that follows the velocity of the fluid is calculated.

$$\dot{V} = vA_{el} \qquad \text{(eq 39)}$$

In the previous equation $\dot{V}$ is the volumetric flow, v is the fluid speed and A_{el} is the area of the cross section of the pipe. Considering that the cross section is eliptical and the two semiaxis are 7 and 1.75 millimeters the obtained velocity is of 0.86615 m/s.

The others normalized parameter of the panel and of the external environment assumed to study the PVT are:

1. The irradiance is considered with a value of 900 W/m^2 and the ambient temperature is considered 305 K (normal values in the month of August in Lisbon, Portugal); [19]
2. The reflector has concentration factor equal to 1,7 and the radiation is evenly distributed on the receiver;
3. The speed of the wind is equal to zero;
4. There are no objects who project their shadow on the receiver;
5. The water circuit is open, therefore a inlet temperature is fixed and the exit temperature depends only on the conditions in the panel;
6. The water circulates with a constant pressure and velocity along the pipe.

The conditions just described idealize the panel; in fact in the real conditions the radiation is not uniform in the back of the receiver, the panel is subjected to the shadings produced by his own structure in some hours of the day.

During the simulation was also introduced another simplification, in fact the PV cells and the conductor are neglected (in the geometry) due to their small depth when compared with rest of the components and the heat production is considered in the silicone simulating the effects of the cells.

The following paragraphs show the simulations obtained using the equation described before. In the first simulation was considered a stationary system and the physic method used were the heat transfer in solid and in fluid. In fact, the fluid flow physics has been simplified (not using the dedicated mechanics but defining simply the fluid and the velocity field as in the annex) due to the increased complexity and to the difficulties encountered later when the flow was imposed has counterflow. Moreover, since the collector is composed of two identical receivers the studies were performed only for one of the two supposing the differences in performance and conditions is negligible.

5.3 Steady-state simulations

To evaluate and progress with the simulation on the collector, produced by the Swedish company Solarus AB, the first simulations were performed with steady state conditions like it the thesis written by Pedro Alves [35]. In particular the 3D simulations made in the previous study were also reproduced because the supposed convective heat transfer coefficient was different. In addition to this studies new studied were performed adding new fluid flow solution (the counterflow fluid) and then studying time-dependent studies.

The steady-state simulation was performed, to compare the situation already studied in the previous thesis (that was also the solution adopted by Solarus AB) also for a new possible solution to refrigerate the collector; the counterflow direction of the water in the conducts. In particular the counterflow studied considered a alternate direction of the flow in the eight pipes. The Figure 26 that follows show the temperature in the receiver top side with the flow in cocurrent (a) and in counterflow (b). The radiation was considered hitting the top and the right side (Figure 26) for the non-concentrated radiation and on the bottom and right side for the concentrated one.

Is important to notice how in the images above and below the scale of the colours shown is modified to improve the visibility of the temperature differences in the surface.

In the image above is clearly visible how the counterflow is more performing having lower temperature than the cocurrent. Moreover, in the image of the receiver with counterflow is clear the effects of the alternated inlet; in fact the points were the inlets are situated are surrounded by a blue area that indicates a colder area. It's important to underline that for this simulation the circuit was considered open therefore the inlet temperature are the same and are indipendent from other parameters. The final consideration that can be made observing the images of the top part is that the right side of the panel reaches higher

temperature than the left side. This can be explained considering that the right side receives also the radiation from the vertical face.

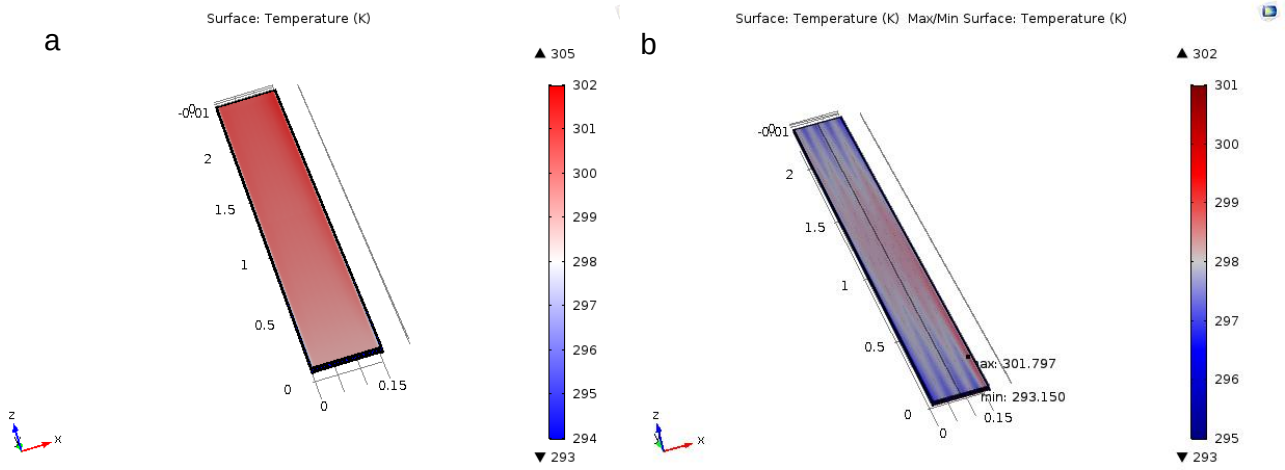

Figure 26 Temperature on the top of the receiver with the fluid in one direction (a) and counterflow (b)

In the picture shown above, Figure 27, can be noticed that the observation made for the top part are valid also for the bottom part.

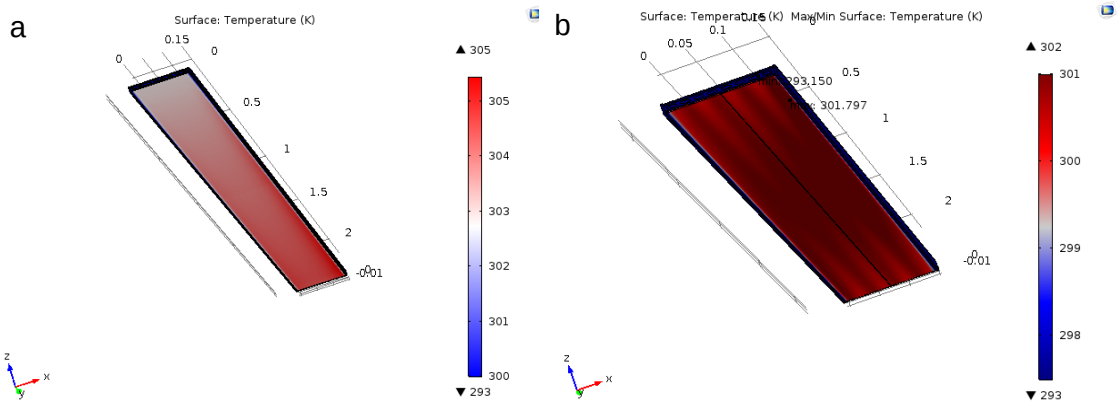

Figure 27 Temperature distribution in the bottom of the receiver with the water flow in in one direction (a) or in counterflow (b)

It can be noticed also that, even if the proximities of the inlet the temperature is obviously colder in the counterflow option this temperature is of the order of the 300 K. On the other hand it almost reaches the 303 K in the single direction solution. As explained in the previous chapters this variation of temperature in the top an bottom part have an impact on the electric efficiency of the collector, therefore the reduction in temperature improve the PV performance.

On the thermal side the thermal efficiency is dependent on the temperature of the fluid that is shown in Figure 28; for the single direction fluid, case a, and the counterflow, case b.

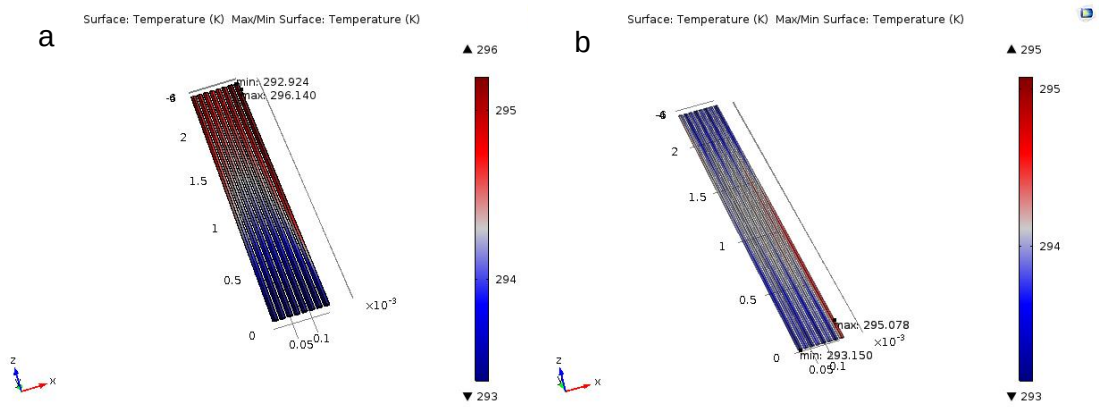

Figure 28 Fluid temperature in the receiver for the single direction flow (a) and for the counterflow case (b)

In the image can be seen how the difference and not uniform temperature is more characteristic of the single direction flow. However, even if this difference in temperature is reflected in the surface and gives a worse electric efficiency, the energy collected in the water is higher and the thermal performances are better in cocurrent flow. The bigger difference in temperature between the inlet and outlet in the single direction flow (visible in the picture above) has a direct influence on the energy harvested by the water that, as explained in the previous part of the thesis, depends on this variation.

These results underline how, many times, the improvements in the energy gained in form of heat and the energy obtained in for of electricity are competing. In fact, the increase of one can decrease the performances of the other aspect. As a matter of fact, the water needs higher temperature in the receiver to increase its performances but the efficiency of the solar cells decrease with this increase. Therefore the compromise between thermal and electric energy have to be decided according to the needs of the location where the collectors are installed. The latitude of the location where the collector is installed becomes, due to the previous considerations, a fundamental parameter in order to decide which one of the two solution is more convenient. In locations with high latitude, like in Sweden, could be more convenient to increase the thermal energy harvested; while on the other hand in countries like Portugal, can be more useful to gain energy in form of electricity.

5.3.1 Thermal effects on the electrical efficiency in a stationary system

Since the purpose of the thesis was decided to be focused on studying the effect that the temperature has on the PV cells, this paragraph shows more in details the electric efficiency variation along the panel.

The following image show the development of the efficiency in the longer axis of symmetry for the single direction flow, Figure 29 a, and for the counter flow, Figure 29 b. Considering that the solar cells are not situated in the surface of the panel the temperature used to calculate the efficiency is the one in the middle of the silicone. The efficiency simulated in figure 29 and 31 are not reflecting the perfectly the efficiency profile that is the minimum one in the cells in series between two diodes and which depends on from the shape of the electric conductor in the single cell. However, this efficiency distribution gives us informations on which parts of the panel are performing better and therefore on how to optimise the diodes distribution and the shape of the electrical conductor.

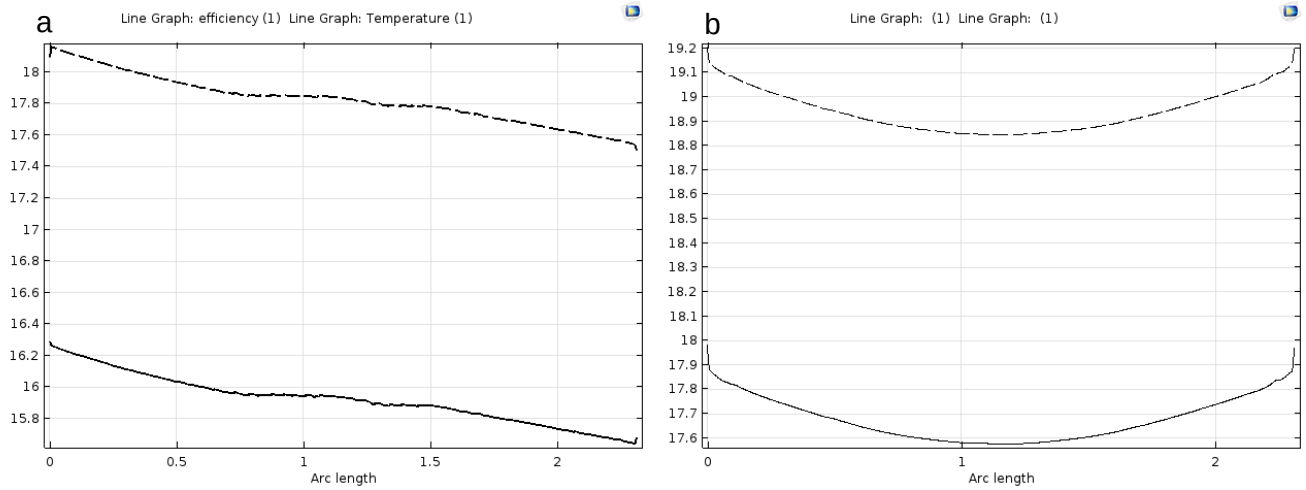

Figure 29 Efficiency on the longer axis of symmetry for the single direction flow (a) and the counter flow (b) cases. In which the dashed line represents the top side and the continuous line is the bottom side.

From the figure above can be seen how the electric efficiency in the single direction flow has a maximum that is smaller than the minimum of the efficiency in the counterflow. Moreover, can be seen that in the first case the efficiency is decreasing along the receiver; while in the counterflow case the efficiency as a parabolic shape. The slight asymmetry noticeable in the counterflow image can be explained considering that also the radiation received is asymmetrical, in facts it reach only one vertical side, and the position of the inlet closer to the irradiated vertical side is at the end of the receiver.

Comparing the graphs of the efficiency with the graphs of the temperature in the same axis, shown below, is possible to notice the symmetrical developments of the efficiency and the temperature.(Figure 30)

The Figure 31 that follows shows the efficiency in the two cases of fluid flow in the short axis of symmetry. It's clearly visible a similarity in the shape of the graphs, however the values of the counterflow, as expected, are higher.

Moreover, can be seen that the solution with the fluid flowing only in one direction has a reduction in the left side that the other solution does not have; this reduction is caused by the better cooling of the central part of the receiver due to the facts that the pipes at the same point have more similar temperature (this is not valid for the other solution). Therefore the sides, that are less cooled, show a decreased efficiency.

The last thing that we can notice from the Figure 31 is the decrease in efficiency for both the solution in the right side. As already said before the irradiation is not completely symmetrical and the asymmetry in the right side of the pictures are originated by this difference.

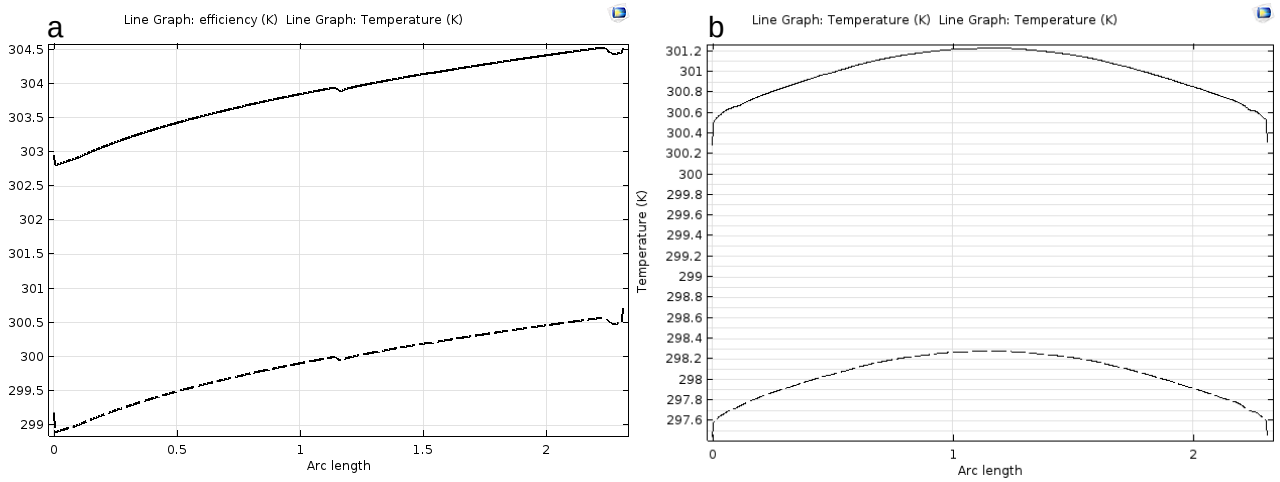

Figure 30 Temperature development along the long axis of symmetry for the single direction flow (a) and for the counter flow (b). In which the dashed line represents the top side and the continuous line the bottom side

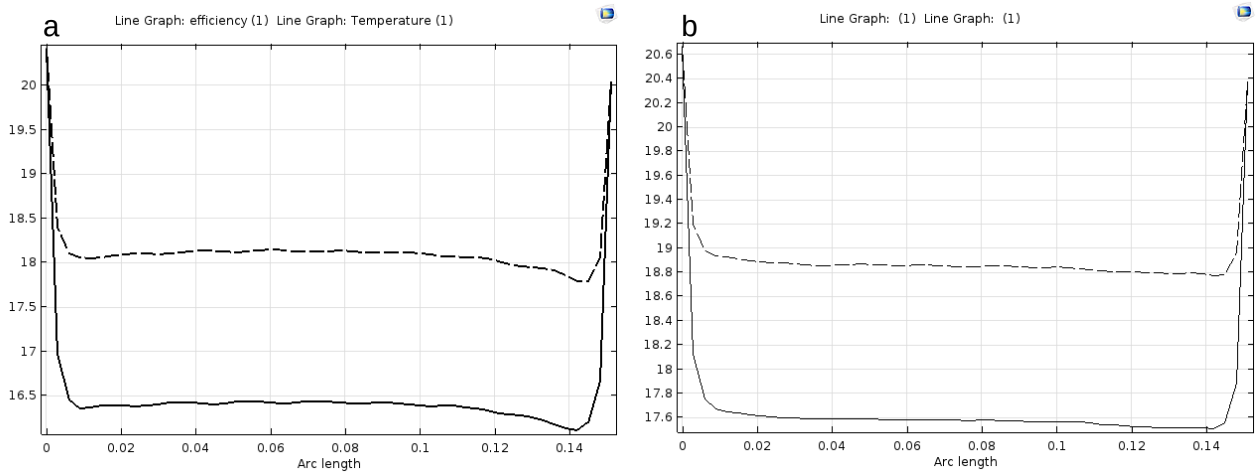

Figure 31 Efficiency development along the shorter axis of the receiver for the solution with the fluid flowing in one direction (a) and the one with the counter flow fluid (b). In both the cases the dashed line represents the top side and the continuous line the bottom side

Comparing the profile of the efficiency in the short axis with the profile of the temperature in the same axis it is possible to see a symmetry in the shapes obtained. Moreover, from the temperature in the middle of the receiver (Figure 32) is possible to notice that the temperature decreases in the water and has its minimum in, for the counterflow, in the centre of the first pipe; while when the fluid flows is only in one direction the centres of the pipes has the warmer water.

The last data that we can extract from the simulation is the electric power produced. It's possible to obtain from the program the average electric efficiency of the two sides of the panel. The results are, in the first case, 18.13% in the top side and 16.47% in the bottom side with an electric power of 144.75 W over a total of 962.89 W received. In the counterflow solution the average efficiency obtained in the photovoltaic part are: 18.97% in the top part and 17.72% in the bottom part; this produces an electric output of 154.05 W.

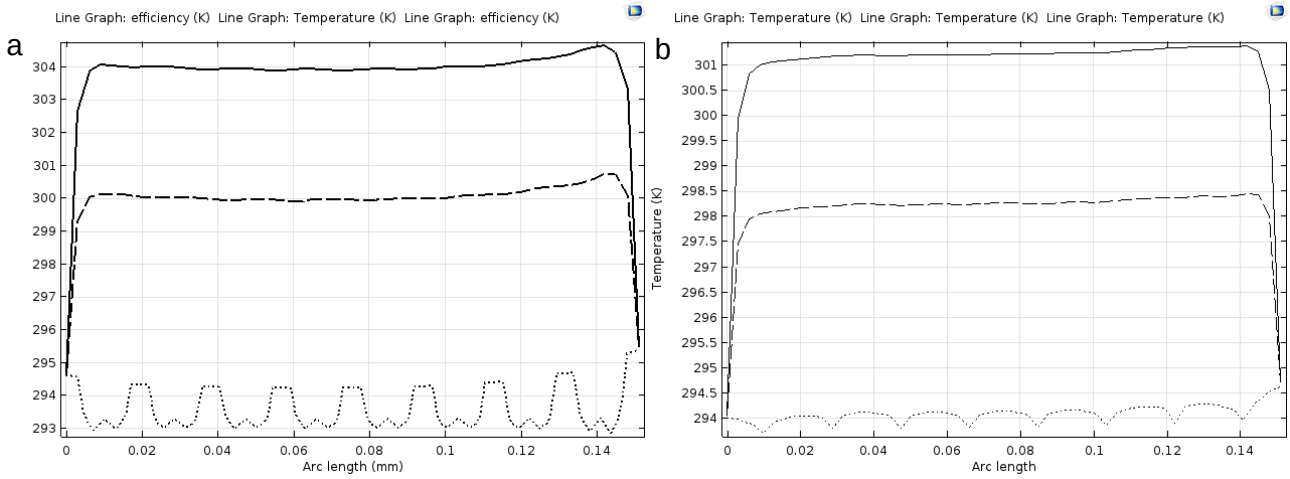

Figure 32 Temperature development in the short axis in the single direction flow case (a) and in the counterflow case (b). In which the continuous line shows the top temperature, the dashed line shows the bottom temperature and the dotted line displays the middle temperature.

6 Time-dependent studies

In order to study if the stationary study ever occurs in the real functioning of the panel and to learn how to introduce time-dependent variable (that can be used also in other studies to study temporary phenomena); the previous simulation were repeated with a irradiance variable with time.

The irradiance studied was equal to the one considered in the stationary studies only in one instant, considered the peak. The time evolution of the irradiance was defined as a Gaussian curve to simulate the movement of the Sun during the day; at the peak the irradiance has the same value of 900 W/m^2 as in the previous studies. The Gaussian equation is generally defined with the following formula.

$$f(t) = ae^{-\frac{(t-b)^2}{2c^2}} \qquad \text{(eq 40)}$$

Where a, b and c are real constant and t is the time in minutes. The constant a indicates the value of the maximum, the constant b the position of the peak and c controls the standard deviation and so the width of the curve. In the simulations conducted a was equal to 1, because then the function was multiplied by the value of the stationary irradiance, b was 360 (the peak was imposed after 6 hours, 360 minutes) and c was 120 (that means that is supposed that the 68% of the radiation is sent in 240 minutes, 4 hours). The Figure 33 below shows the obtained gaussian distribution as function of the time.[36]

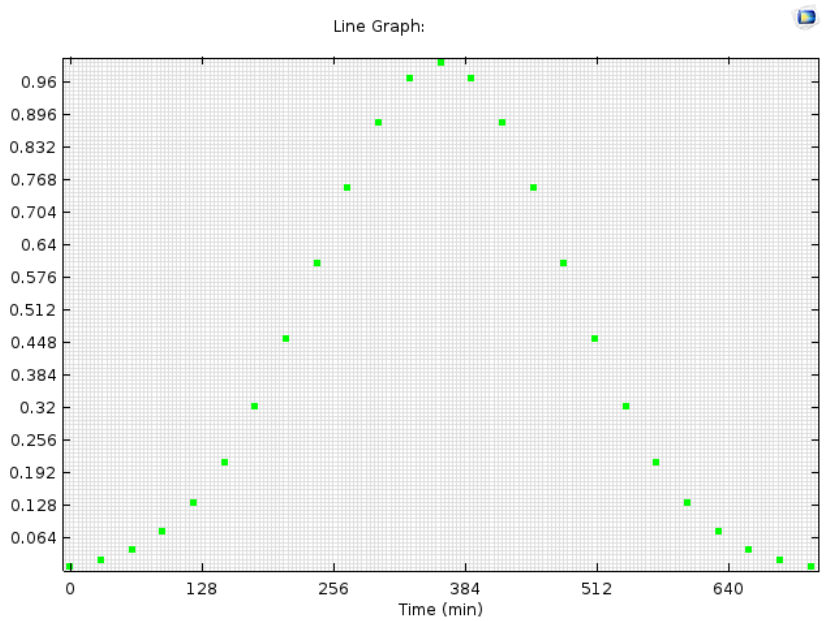

Figure 33 Gaussian distribution as function of the time

6.2 Result analysis for a time-dependent simulation for the counterflow solution

After the simulation it is possible to analyze the development of the temperature, the efficiency and all the other parameters during the length of a day.

In the figure below is shown the development of the temperature on the top of the receiver with time.

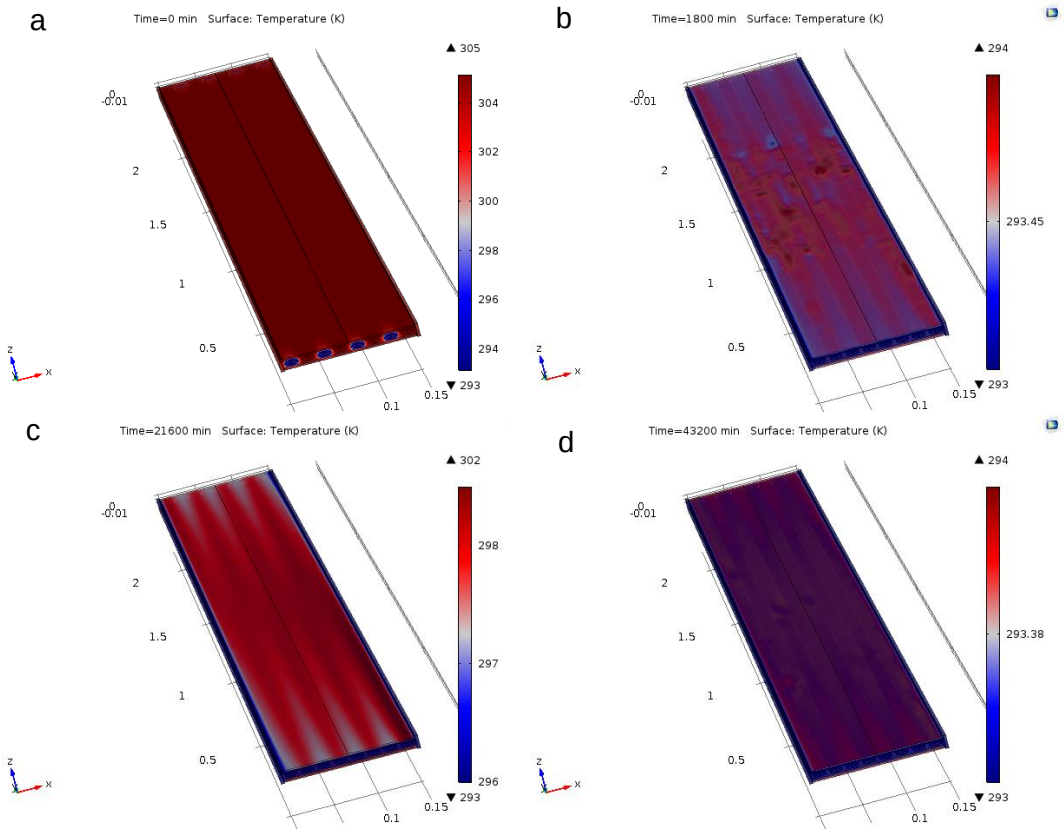

Figure 34 Time progression of the temperature in the top side of the receiver in a counter flow solution. The times analysed are: 0 minutes (a), 30 minutes (b), 360 minutes (c), 720 minutes (d)

From the development of the temperature it's possible to notice that the receiver is rapidly cooled and the temperature distribution drops until when due to the increasing irradiance rises again and reaches is peak point after 360 minutes. To understand in a better way the results and reduce the confusing effects of the grid distortions (visible in the images as spots of more irregular temperature in the same areas of the receiver with the passing of time) the range of temperature displayed with a different colour has been modified. Modifying the visible data means that the temperatures that are higher and lower of certain values are visualized with only two colours without shades. The effects of the irregularities in the mesh are reduced with the passing of time in facts the area affected decreases because the more

distorted elements of the mesh become similar in results to the other mesh components of the simulation. The Figure 35 that follows shows an example of distortion in the mesh.

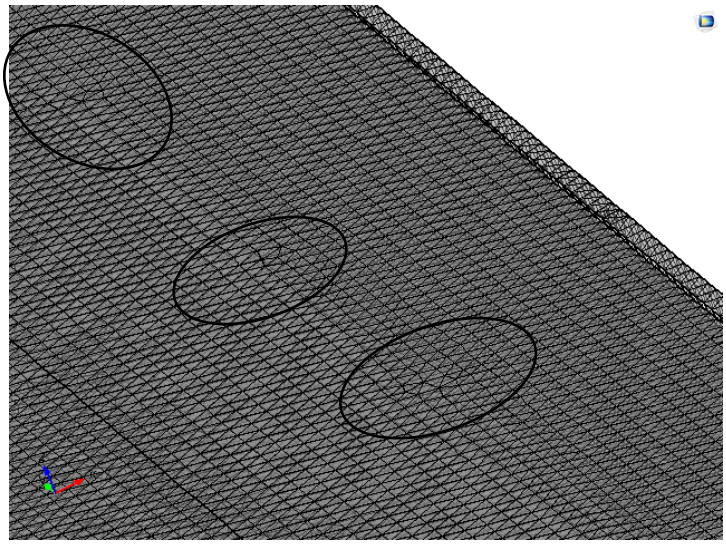

Figure 35 Example of mesh distortion in the simulation program

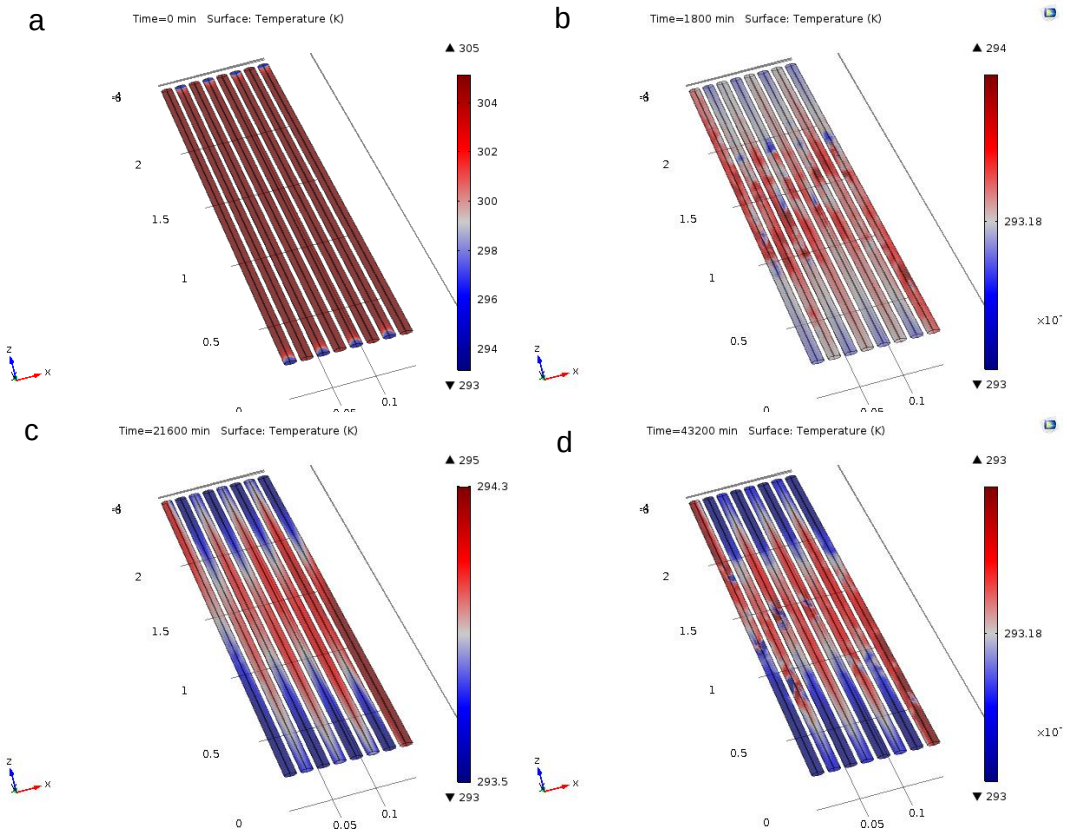

Figure 36 Time progression of the temperature in the fluid in the receiver in a counter flow solution. The times analysed are: 0 minutes (a), 30 minutes (b), 360 minutes (c), 720 minutes (d)

Excluding the effects of the mesh asymmetries, the results present a distribution of temperature similar to the one obtained in the stationary simulation. In facts, the receiver has a lower temperature in

proximity to the water conducts. The similarities in the temperature distribution can be appreciated also in the fluid as displayed in Figure 36 above.

Also in the fluid temperature distribution are visible the effects of the mesh irregularities and the similarities with the temperature distribution in the stationary study. The study of the temperature in the fluid is important because the difference of temperature between inlet and outlet, as explained in the previous chapter, is a key parameter to evaluate the thermal power obtained. From the images above is clearly visible that the fluid temperature varies a lot during the twelve hours simulated, with a maximum difference around 3 K in the peak point and a minimum difference very close to 0,1 K in the last moment. However, since both in the fluid image and the receiver image the quantitative evaluation of the temperature is difficult the Figures 37 and 38 were introduced to show the evolution in time of the temperatures in the two symmetry axis.

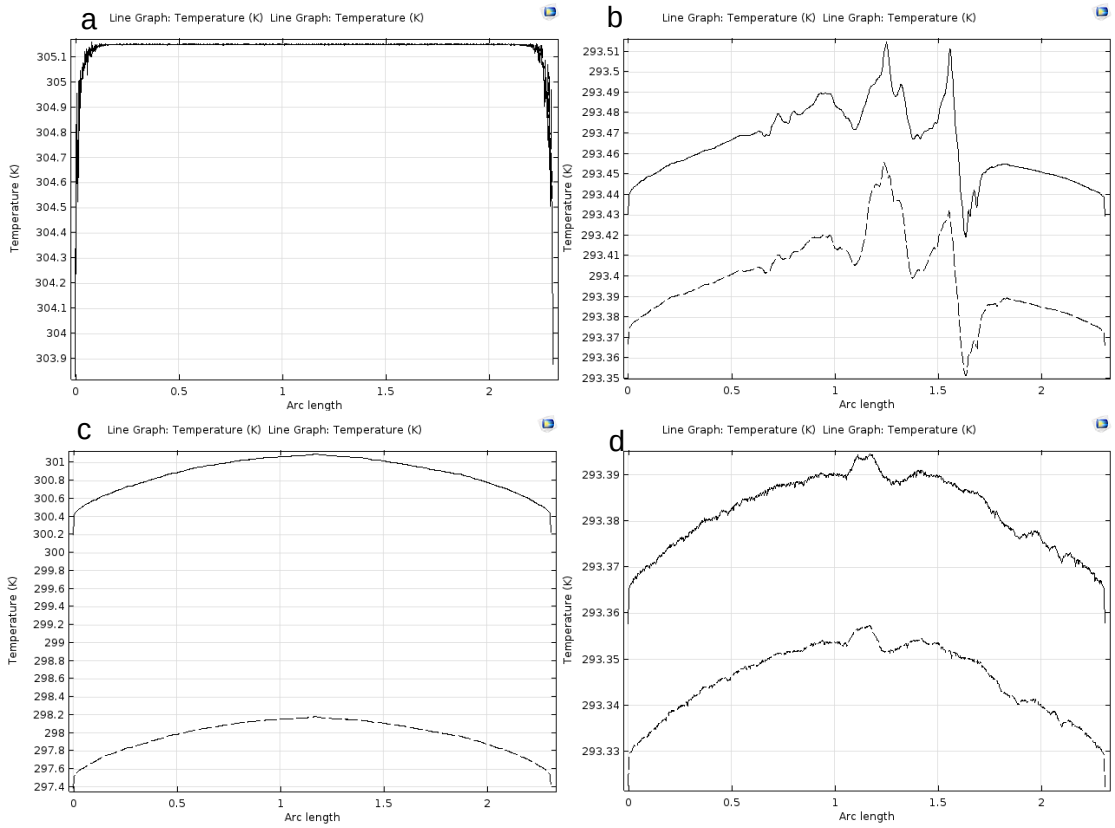

Figure 37 Time progression of the temperature in the long symmetry axis in a counter flow solution. The times analysed are: 0 minutes (a), 30 minutes (b), 360 minutes (c), 720 minutes (d). The dashed line represent the top side and the solid line represent the bottom side

The graphs above are showing how during the time the program reduces the effects of distortion. However, comparing the images c and d is possible to notice that the bigger difference of temperature produces also a more sharp temperature distribution, reducing the effects of distortions. Analysing the shape of the temperature in the long axis is possible to notice a parabolic development along the length similar to the one obtained under stationary conditions.

From the first frame of Figure 38, that follows, is possible to see how the program starts the simulation. In fact even if the input data impose a certain temperature the simulation introduces perturbations due to the micro-system that are solved during the computation and due to the interaction between the different elements with different temperature.

Considering the information obtained from both the two axis we can suppose that the counterflow solution gives a more homogeneous distribution of the temperature producing a bigger symmetry both in the direction of the longer axis and in the direction of the short axis. In the single direction flow the hottest area is normally in the centre (with the exception of the area surrounding the most right pipe) and not in the end of the receiver like in the other solution

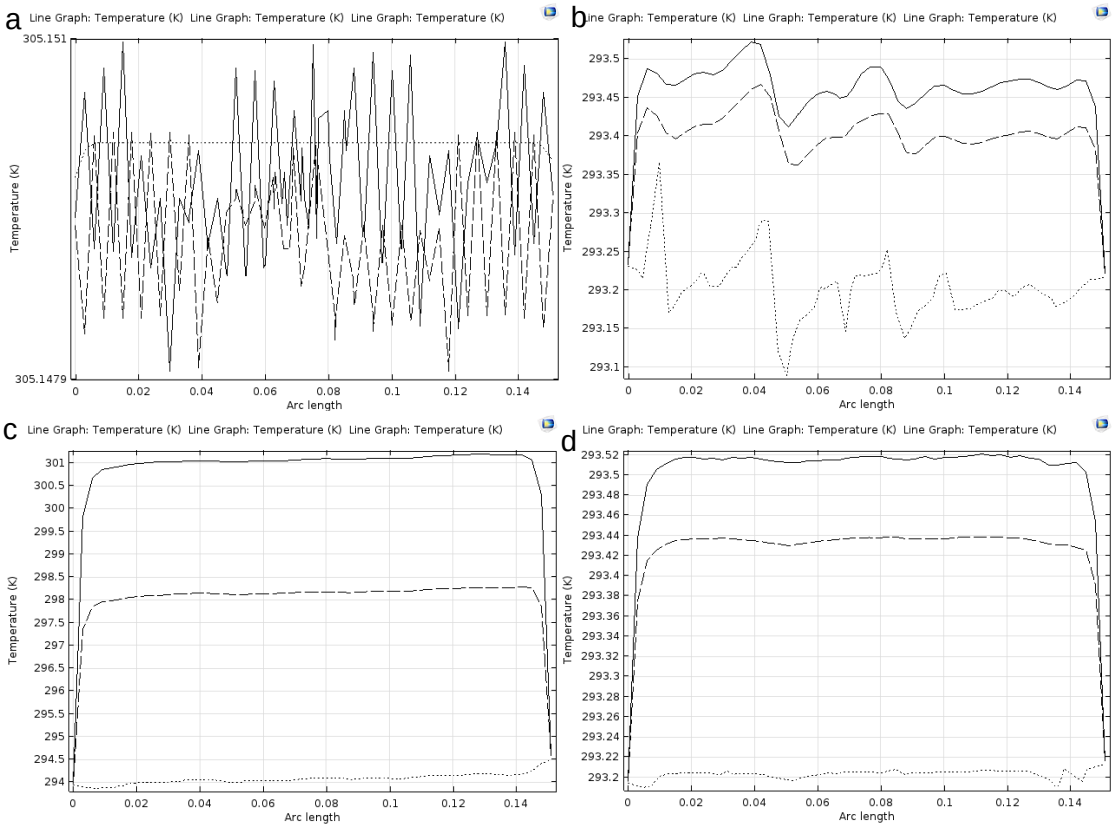

Figure 38 Time progression of the temperature in the short symmetry axis in a counter flow solution. The times analysed are: 0 minutes (a), 30 minutes (b), 360 minutes (c), 720 minutes (d). The dashed line represents the top side, the solid line represents the bottom and dotted line is the middle temperature.

Analyzing the variation of the average efficiency during 12 hours of operation, Figure 39, it is visible how the performances of the top PV (in blue) and the bottom PV (in orange) are similar when the radiation is low. In facts in these points the temperature difference is lower, but in the peak point they have different efficiencies.

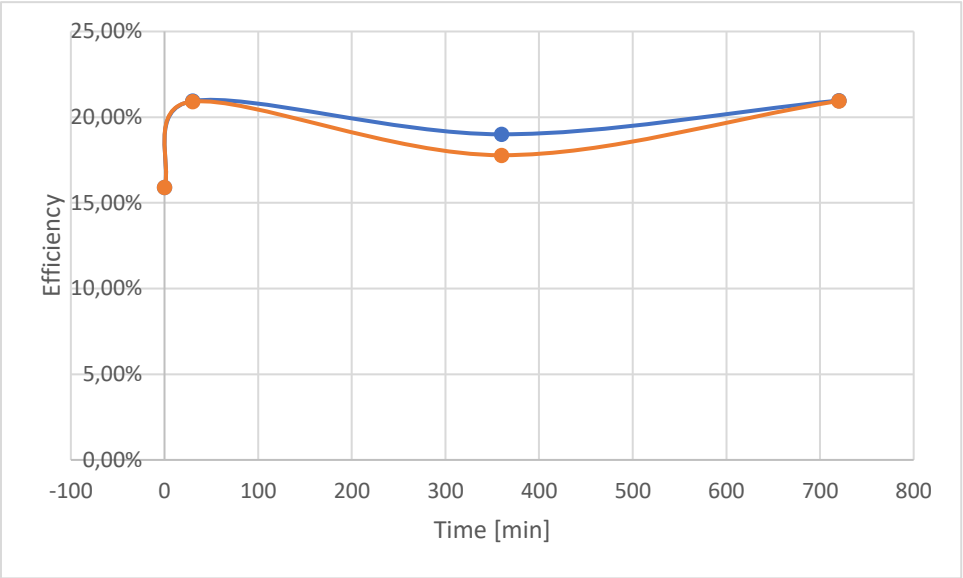

Figure 39 Average efficiency in the PVs during 12 hours. The PV on the top side is represented in blue while the bottom one in orange.

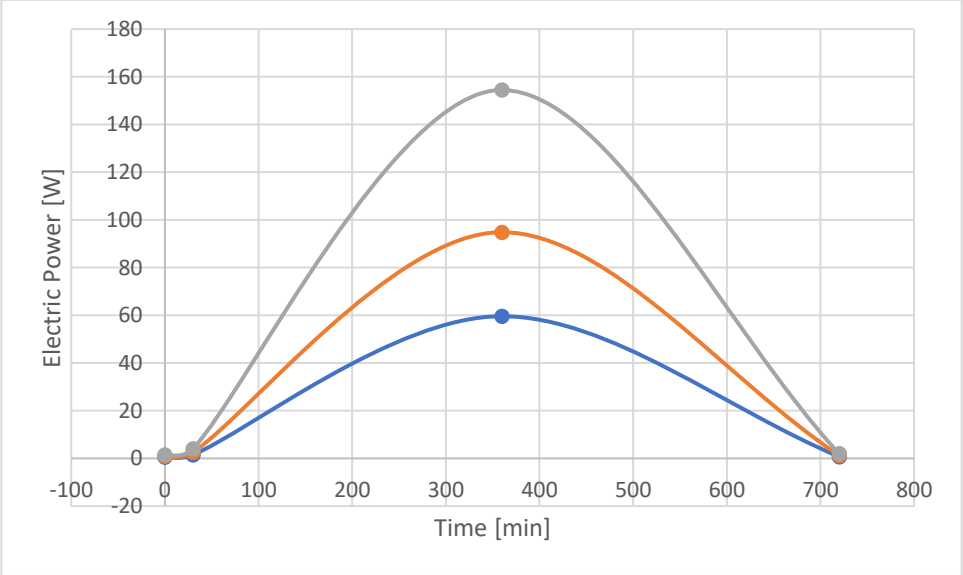

Figure 40 Electric power output during the time divided by top PV (in blue) bottom PV (in orange) and total (in grey)

As expected is possible to notice, from Figure 40, that the output follows the shape of the irradiance. However it clear that thanks to the concentration of the light in the bottom the electricity production is higher in this side even with a lower irradiance.

In the picture below is possible to see that the concentrated power represents more than the half of the total power received. This shows, together with the previous image, that the effects of the concentrated light are more positive than negative.

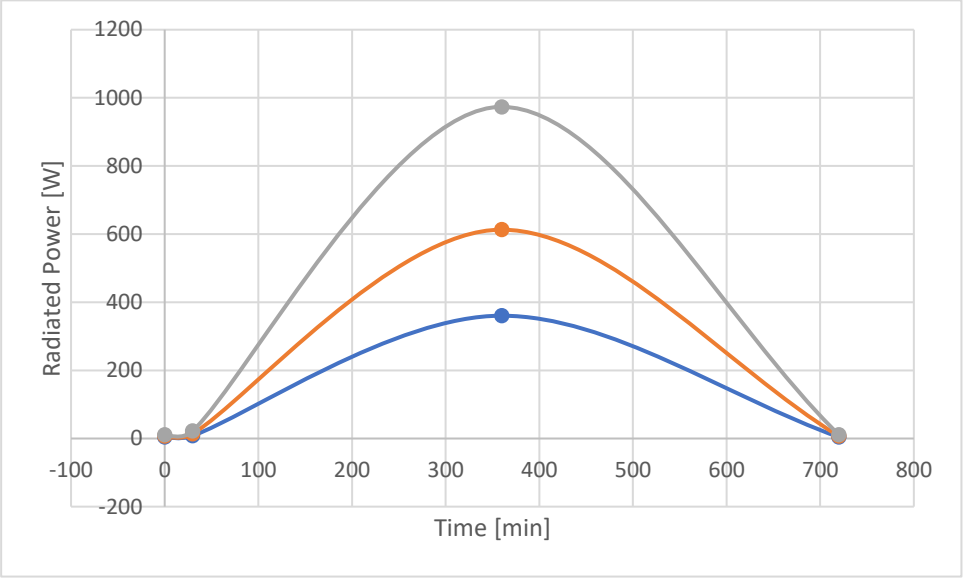

Figure 41 Power received by radiation during time show as normal radiation (in blue), concentrated radiation (in orange) and total radiation

6.3 Result analysis for a time-dependent simulation for the cocurrent solution

Since the result produced by the counterflow solution revealed that the stationary condition are a limit case, that never really happens, the time-dependent simulation was simulated also for the single direction flow.

In a similar way to the counterflow solution is visible by the analysis of the temperature profile that the stationary conditions bring to an non-realistic solution. The actual temperature is kept lower by the constant flow of water and the variation of the irradiance impedes to the receiver to increase in temperature until the stationary levels. In Figure 42 is possible to notice how, starting the simulation with a temperature similar to the one obtained as result of the stationary study (305 K), the temperature rapidly drops reaching values similar to the one of the fluid that enters in the receiver. In a second moment due to increase in irradiance the temperature grows until the half of the time where the power received reaches its peak. In the peak point, shown in Figure 42 c, the temperature has a maximum of around 301 K that is still lower than the temperatures reached in the stationary condition where the peak was around 306 K.

From the images is clear that the temperatures are very similar in some moments, moreover to understand in a better way the results and avoid the confusing effects of the grid distortions, like in the previous case, the range of temperature shown with a different colour has been modified. The progression below shows how the program corrects the effects of the grid distortion with the passing of time and how, as expected, the temperatures are higher closer to the outlet. Since the temperatures

obtain are not very quantitative clear in the image in Figure 43 was displayed the temperature variation in the long axis.

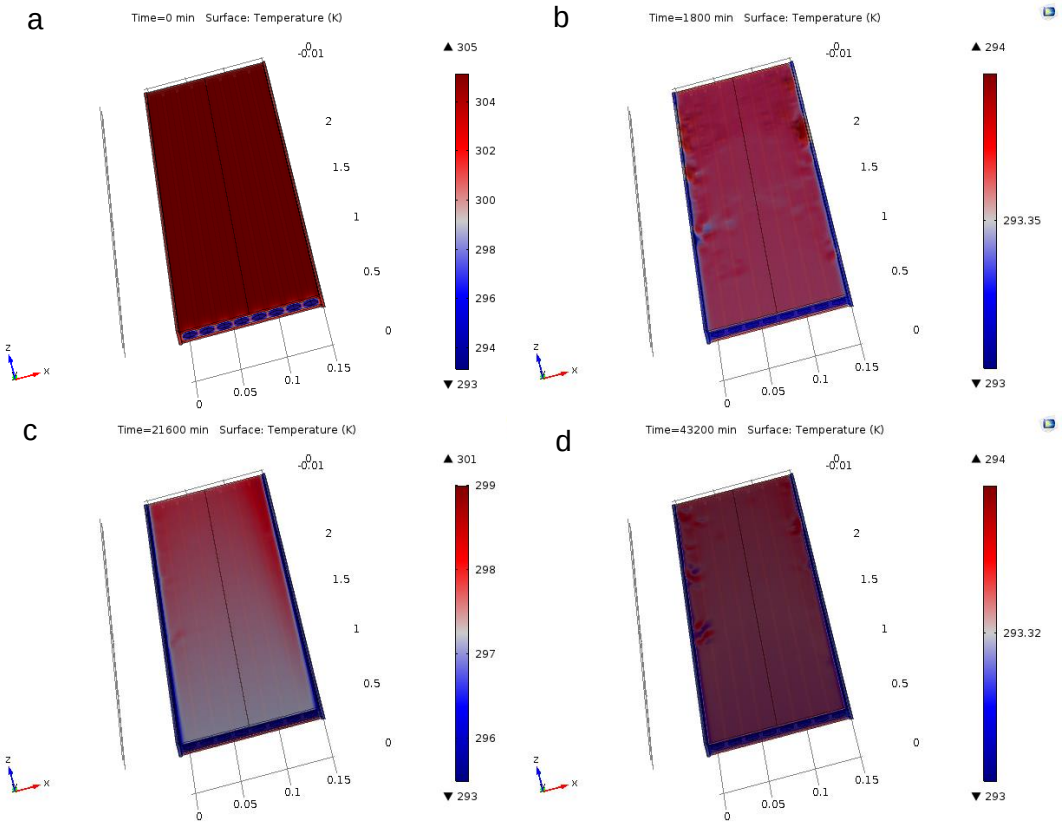

Figure 42 Time progression of the temperature in the top side of the receiver for the one direction fluid solution the times analysed are: 0 minutes (a), 30 minutes (b), 360 minutes (c), 720 minutes (d)

Figure 43 shows how the difference in temperature between the top side and the bottom side increases with the increasing irradiance, it is about 3 K at the peak point while only 0,3 K in the last point. The second observation that can be made from the graphs is that the irregularities are surpassed with the passing of time and with the higher irradiance, in fact they are bigger after 30 minutes but in the last two time section they are almost not existing.

Comparing Figure 43 with the results of the counterflow it is possible to see that the obtained images are not in line with the expectation produced in the stationary case. In facts, the distribution of temperature obtained is similar to the one of the stationary case but the values remain lower than those of the counterflow. This unexpected result can be caused by a mistake in the parameter imposed to the simulation or by a assumptions that are revealed not valid.

One of the supposition, that can be done, is that the response of the system to the variation of the irradiance is not fast enough to reach the configuration obtained in the stationary case. However at the moment of the end of the thesis the cause of this problem was still not solved.

If the supposed reasons of the surprising results will be confirmed the speed of the change in the different phenomena becomes a crucial parameter to identify the relevant perturbation in the functioning of the panel during its lifespan.

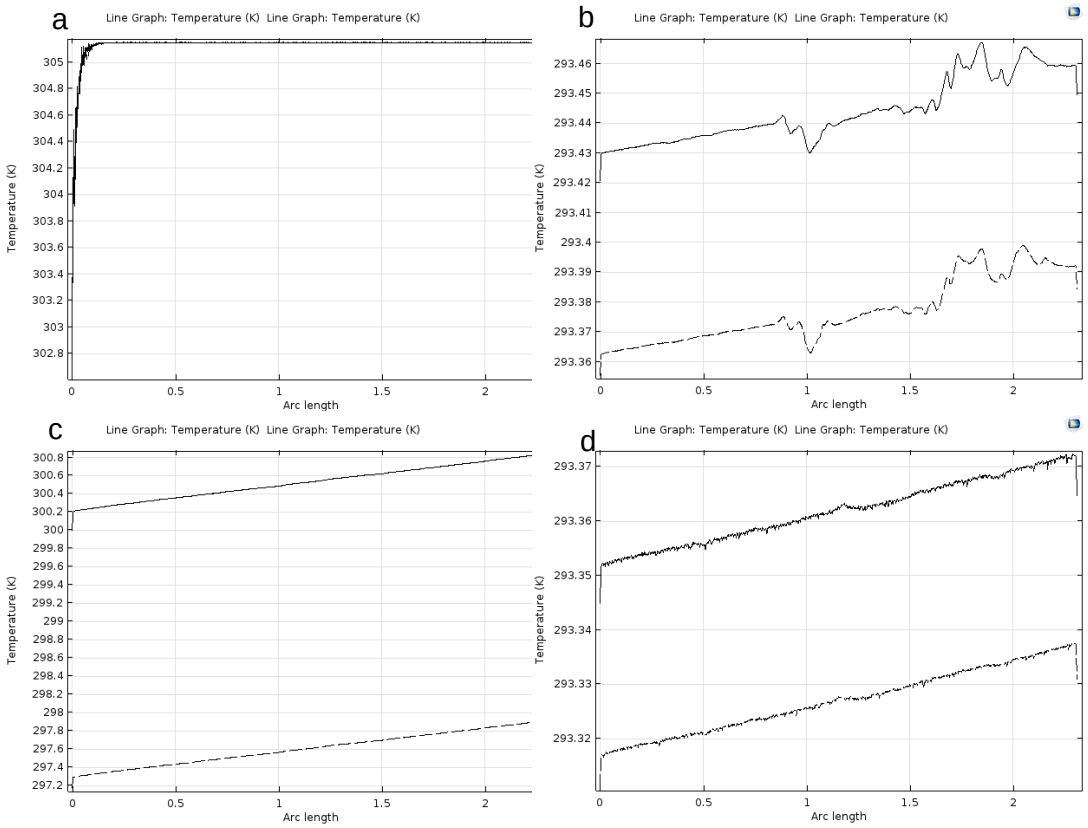

Figure 43 Time progression of the temperature in long axis of the receiver for the one direction fluid solution. The times analysed are: 0 minutes (a), 30 minutes (b), 360 minutes (c), 720 minutes (d). The solid line represents the temperature of the bottom of the receiver while the dashed line shows the temperature of the top side.

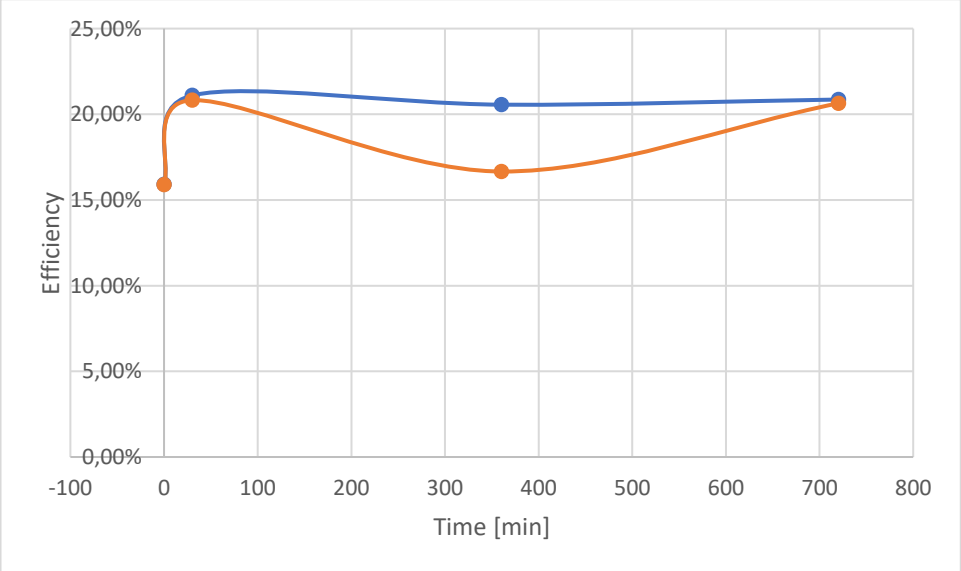

Figure 44 Average efficiency in the PVs during 12 hours in the single direction solution. The PV on the top side is represented in blue while the bottom one in orange.

The average efficiency on the two PV panels like in the previous solution, the counterflow one, is more similar when the irradiance is lower. However, at the peak of the irradiance the top PV, represented by the blue line in figure 44, has a very small drop of efficiency. On the other hand, the drop at the maximum irradiance in the bottom PV, the orange line in figure 44, is higher than the drop seen in the counterflow case. The negative effect more visible in the bottom PV is visible also in the power output shown in the figure 45.

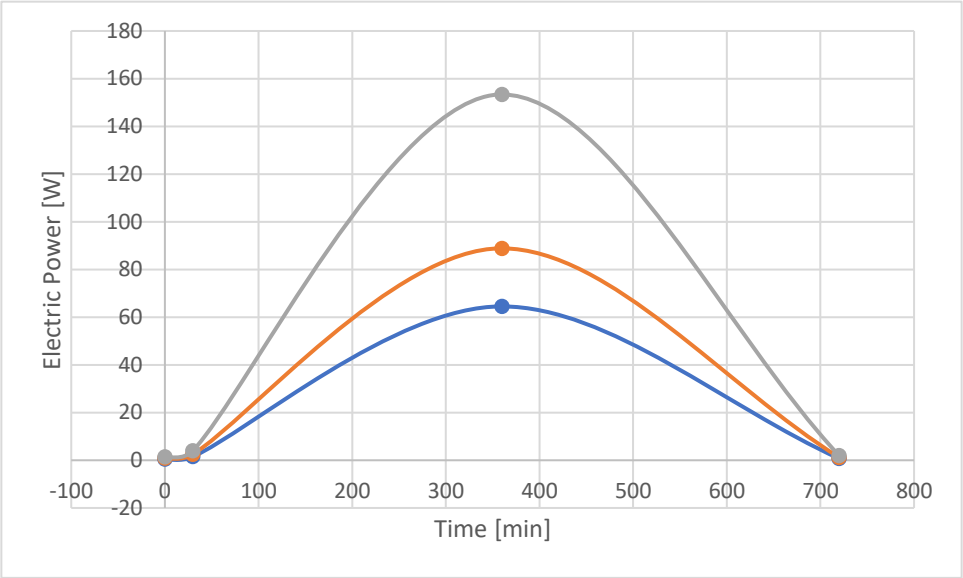

Figure 45 Electric power output during the time in the cocurrent case; divided by top PV (in blue) bottom PV (in orange) and total (in grey)

The electric power output with the passing of time in the current case, figure 45, make us see how the total power output (in grey) is similar to the one obtained for the counterflow case shown before. However, the power coming from the bottom side (in orange) is smaller than in the previous case and the power produced by the top side (in blue) is bigger.

This results as for those of the temperature distribution analyzed before are unexpected. In fact, from the stationary case was expected a lower efficiency than the counterflow case and therefore a smaller power output.

7 Conclusions and possible future developments

The effects of the external environment are of crucial importance when analyzing the performances of a solar collector or a photovoltaic panel. Therefore, it becomes even more important when an hybrid system is taken into account due to the required compromises needed to manage this two technology together.

The two most important parameter are the irradiance and the temperature that have an effect both on the thermal and the electrical part. In fact, in the electrical part the short circuit current (I_{sc}), the open circuit voltage (V_{oc}), the maximum power current (I_{mp}) and the maximum power voltage (V_{mp}) are dependant on two factors influenced by the temperature: the inverse current of saturation (I_0) and the thermal voltage (V_T). In the thermal side of the system the temperature in the fluid, in this case the water, is responsible for the performances and the efficiency as shown in the third chapter.

The computational simulation, as those studied in this thesis, are becoming more and more important in the development and the design of many different products. This tools in fact are improving in the last years and are creating a new an cheaper way of testing and trying new ideas or, in the case of this thesis, new configurations. Moreover, these simulations increase the speed at which the new tests can give results. In facts, they can simulate a phenomenon in a time shorter than the real time needed for an experiment. Other strength points are the possibility of obtaining valid result without having the real objects (reducing the costs and the spaces used) and the possibility of using condition otherwise very difficult to obtain; for example from Portugal is possible to simulate the behaviour of a panel in Sweden.

In this thesis the focus was given in chapter six to the introduction of a different solution for the cooling that was not studied before for the product, given by the company Solarus AB, in the previous studies. This new solution was the introduction of a counterflow of the water in the conducts of the receiver. Already in the first simulation, in stationary condition, was clear the difference obtain in the temperature of the photovoltaic panels cooled in a better way and therefore with a more uniform and lower temperature. The lower temperatures obtained in the PV cells are responsible for the positive change in the efficiency of the electrical part, that benefits from these new conditions. In the thermal part, however, due to the lower temperature of the fluid that comes out, the power output is reduced.

These first results already suggested that the adoption of one of the two solutions can be dependent on the latitude and the conditions of the single installation. The adoption of a collector more performing in the photovoltaic part can be, in facts, more convenient in a situation where the energy in form of heat is less needed. In latitudes with higher irradiation can be more convenient considering the installation of a CPVT to produce more electricity and another system dedicated to the production of heat.

The following development of the thesis introduced the time-dependent studies. This was done in order to proceed with simulation more and more similar to the condition that the collectors are facing once that they installed in the different locations. However, even if these simulations some simplifications and

idealization need to be made; to maintain the possibility of comparing the results with the previous study and to avoid to exceed the hardware possibilities.

The simulations performed in the chapter seven supposed a variation of the irradiance that describes a Gaussian bell during twelve hours. The results of these simulation shows that the configuration of the stationary simulation are never reached, even in an idealized system. Moreover they presented some results that need further studies, in facts the cocurrent solution had lower temperature than the counterflow one. One of the proposed explication for this results was that the time of response of system is different for the two options. Therefore, even if both do not reach the stationary situation, when the fluid goes in one direction the temperature remains lower.

This study demonstrate the advantages of the virtual simulation permitting to obtain new developments without changing the geometry of the receiver, saving time and reducing the costs. These new developments open the way to new possible studies that were not performed in this thesis because of limits of time and hardware.

These studies could be the introduction of the shadings in the time-dependent studies to analyzed in future works possible critical situation. One of this shading studies would be the study of the shading that the structure produces on the receiver in the firsts and lasts minutes of irradiation.[27]

Other interesting studies that could be done in the future could involve a time-dependent variation of the fluid flow that balances the variation of irradiation during the day. However, this studies should also consider that a variation of the fluid speed produces also a variation in the costs that need to be taken into account.

Other more simple studies can involve a variation of the materials that create the receiver. To study the different compromises between the costs of production and the performances obtained with the different characteristics of the different material.

References

[1] *D. Carrington, "The Anthropocene epoch : scientists declare dawn of human-influenced age," pp. 1–5, 2016.*

[2] *Solarus AB, THE NEW POWER TO FUEL OUR FUTURE. technical brochure, 2017.*

[3] *"What are the most efficient solar panels on the market ?," 2017. [Online]. Available: http://news.energysage.com/what-are-the-most-efficient-solar-panels-on-the-market/. [Accessed: 07-Oct-2017].*

[4] *"WHAT IS THE MOST EFFICIENT SOLAR," 2017. [Online]. Available: http://www.jojusolar.co.uk/2017/06/06/high-efficiency-solar-panel. [Accessed: 07-Oct-2017].*

[5] *"Panasonic surpasses SolarCity with world ' s most e cient solar panel," 2017. [Online]. Available: http://inspiredevolution.co.za/panasonic-surpasses-solarcity-with-worlds-most-efficient-solar-panel/. [Accessed: 07-Oct-2017].*

[6] *"Breve história da energia solar." [Online]. Available: http://web.ist.utl.pt/palmira/solar.html. [Accessed: 31-Oct-2017].*

[7] *H. Z. Ã et al., "The history of solar," Sol. Energy Mater. Sol. Cells, vol. 93, pp. 1461–1470, 2011.*

[8] *T. Ward, "This is the most efficient solar panel ever made," 2017. [Online]. Available: https://www.weforum.org/agenda/2017/08/this-is-the-most-efficient-solar-panel-ever-made. [Accessed: 07-Oct-2017].*

[9] *D. R. Tobergte and S. Curtis, "Concentrator Photovoltaics." [Online]. Available: http://link.springer.com/10.1007/978-3-540-68798-6. [Accessed: 31-Oct-2017].*

[10] *A. A. Rahman, "Master Level Thesis Electrical Evaluation of a Low Concentrating PVT Collector.pdf," Dalarna University, 2015.*

[11] *B. A. S., Photovoltaics for Commercial and Utilities Power Generation. 2011.*

[12] *"A single plant, cogeneration of energy, up to 75% of efficiency," 2017. [Online]. Available: http://www.greenetica.com/en/benefits.html. [Accessed: 31-Oct-2017].*

[13] *S. Inc, "The future of parabolic trough technology," 2017. [Online]. Available: http://www.skyfuel.com/products/skytroughdsp/. [Accessed: 08-Oct-2017].*

[14] *"Parabolic trough solar power plants," 2017. [Online]. Available: http://www.dlr.de/media/en/desktopdefault.aspx/tabid-4987/8424_read-20582/.*

[Accessed: 31-Oct-2017].

[15] A. Solartron, HYBRID PARABOLIC SOLAR CONCENTRATOR 9 M. 2017.

[16] S. P. Philipps, A. W. Bett, K. Horowitz, and S. Kurtz, "Current Status of Concentrator Photovoltaic (CPV) Technology," Natl. Renew. Energy Lab., pp. 1–25, 2015.

[17] "Solar Uninterrupted Power Supply [ups] - Power from Sun !," 2017. [Online]. Available: https://sites.google.com/site/solarupssystem/solar-power-generating-ups-is-durable-for-your-home-to-use-computers-and-lights. [Accessed: 09-Oct-2017].

[18] "Solar Power," 2017. [Online]. Available: http://www.alternativeenergyhq.com/best-solar-power-regions-worldwide.php. [Accessed: 31-Oct-2017].

[19] G. Italian, I. E. Agency, S. Heating, C. Programme, and S. Antipolis, "Photovoltaic Geographical Information System (PVGIS) Interactive access to solar resource and Posters and maps of solar resource and JRC â€™ s Directorate C : Energy , Transport and Climate - PVGIS - European Commission," 2017. [Online]. Available: http://re.jrc.ec.europa.eu/pvgis/. [Accessed: 31-Oct-2017].

[20] Comsol, Heat Transfer Module: User's Guide. 2012.

[21] C. Zener, "General Theory of Thermoelastic Internal Friction," in Internal Friction in Solids, vol. 230, no. 1937, 1938.

[22] Kalogirou and Soteris, Solar Energy Engineering: processes and systems. 2009.

[23] D. J. Dunn, "Fluid Flow Theory," no. 1, pp. 1–34.

[24] C. Newtonian, I. Newtonian, T. Navier, and T. Navier, "Derivation of the Navier – Stokes equations," 2015. .

[25] J. Nelson, "Introduction," in The Physics of solar cells, 2003.

[26] R. M. G. Castro, INTRODUÇÃO À ENERGIA FOTOVOLTAICA Rui M.G. Castro, vol. 2002, no. edição 0. 2002.

[27] C. A. F. Fernandes, J. P. N. Torres, J. Gomes, P. J. C. Branco, and S. K. Nashih, "Stationary solar concentrating photovoltaic-thermal collector - Cell string layout," Proc. - 2016 IEEE Int. Power Electron. Motion Control Conf. PEMC 2016, pp. 1275–1282, 2016.

[28] D. Lenardic, "Solar Cells," 2015. [Online]. Available: http://www.pvresources.com/en/solarcells/solarcells.php. [Accessed: 13-Oct-2017].

[29] *E. Skoplaki and J. A. Palyvos, "On the temperature dependence of photovoltaic module electrical performance : A review of efficiency / power correlations," Sol. Energy, vol. 83, no. 5, pp. 614–624, 2009.*

[30] *A. De Simone, "NOCT fotovoltaico e resa dell'impianto," 2015. [Online]. Available: http://www.ideegreen.it/noct-fotovoltaico-57094.html.*

[31] *J. Gomes, L. Diwan, R. Bernardo, and B. Karlsson, "Minimizing the impact of shading at oblique solar angles in a fully enclosed asymmetric concentrating PVT collector," Energy Procedia, vol. 57, pp. 2176–2185, 2014.*

[32] *S. K. Nashih, C. A. F. Fernandes, J. P. N. Torres, J. Gomes, and P. J. C. Branco, "Validation of a Simulation Model for Analysis of Shading Effects on Photovoltaic Panels," J. Sol. Energy Eng. Trans. ASME, vol. 138, no. 4, 2016.*

[33] *"Shading of a Single Cell," 2017. [Online]. Available: http://www.pveducation.org/pvcdrom/modules/shading. [Accessed: 31-Oct-2017].*

[34] *R. S. Lotti, A. W. Machado, Ê. T. Mazzieiro, and J. L. Júnior, "Aplicabilidade científica do método dos elementos finitos," R Dent. Press Ortodon Ortop Facial, vol. 11, no. 2, pp. 35–43, 2006.*

[35] *Pedro and Alves, "Coletor Fotovoltaico-Térmico Estacionário com Concentrador : Análise Térmica Engenharia Electrotécnica e de Computadores Júri," Istituto Superior Técnico, 2016.*

[36] *"Gaussian Function." [Online]. Available: https://en.wikipedia.org/wiki/Gaussian_function. [Accessed: 31-Oct-2017].*

Annex

A.1 First simulations

Before the beginning of the PVT panel simulation it was necessary to learn the language and the possibilities offered by the simulation program; introducing the physical mechanics studied in the previous chapter little by little, namely the functions related to the heat transfer. To simplify, we have used a simple geometry (a pipe in contact with a panel in the bottom of it).

To create the 3D model, it was used the dedicated section of the program, even if the software gives also the option to import a file created with different programs designed for modelling.

Once that the geometry is defined, the program gives to the user the possibility of choosing a material for the different parts among a list of known ones. Alternatively, the user can introduce a personalized material.

In the next step, the program requires the description of the physical phenomena by the inclusion of their specific parameters. In these preliminary studies, two heat transfer modes were used: the first related to solids and the second related to fluids. The program can include different mechanics and consider different starting conditions, especially in the fluid study. In this case, the simulation may take into account the influence of the laminar velocity field on the heat transfer along the several elements of the grid.

In the first simulations, the effect of the sun was modelled by a heat source in the plate, while in the following studies, it was considered that the sun hits the surfaces like a boundary heat source. At this early stage, the main purpose of the simulations was to study the response of the program and to understand the interfaces of sections dedicated to different physical phenomena. Therefore, in this preliminary analysis, the values of the different variables were purely arbitrary. In particular, it was necessary to be sure that the heat was passing from the solid to the liquid in a correct way.

After defining the physics that regulate the simulation, a mesh must be created in order to divide the geometry into the elements that allow the program to run a specific simulation. The mesh in the case of a 3D analysis creates many different tetrahedral elements that fill the geometry studied. The accuracy of the simulation can be regulated by the number of elements. Predefined meshes or personalized meshes, fully customized in dimensions, can be chosen. In this thesis only the predefined meshes were used, except in the test with fictitious geometry, where the mesh used a size defined as normal by the program.

In order to be effective, the type of analysis shall be chose. Different options are available, namely, (*i*) parametric study, (*ii*) time-dependent study and (*iii*) stationary study. For the first analysis, a time-dependent study was chosen.

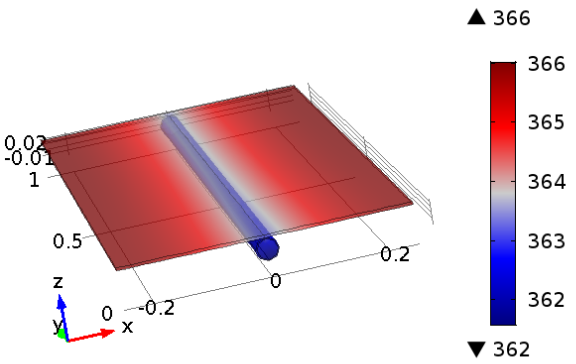

Figure 46 Temperature in the simplified geometry

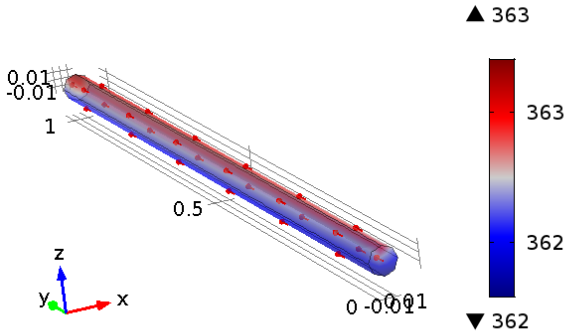

Figure 47 Fluid temperature in the simplified geometry with direction of the fluid (arrows)

After passing through all the previous stages, the program can proceed and execute the simulation towards the results, which will discussed below. The postprocessing mode, offered in the result section of the software, gives us the possibility to manage and show the results in the most effective way, by choosing the colours, creating graphics and tables, customizing the domains displayed and so on. In Figure 46, it is presented the time evolution of the temperature along the domains, while in Figure 47 it is visible the change in temperature that occurs in the water. As expected, the temperature is colder in the pipe than in the plate. Particularly it shall be highlighted that the effect of cooling is stronger in the line where the pipe is in contact with the plate. Analysing the sub-domain of the water in Figure 47, it is apparent that: (*i*) the liquid heats up more and more as it proceeds from the inlet into the direction to the outlet and (*ii*) the portion of the pipe occupied by the hot water (in red) increases.

A.2 Fluid flow simulation

In the second type of simulation analysis, it was studied more in details the fluid flow mechanics, especially the one referred as *laminar flow*.

For that, the geometry used in the simulation was modified: a straight iron alloy pipe for the water flow was used.

The physical methodology introduced was the laminar fluid flow mode. Initial conditions has been clearly defined, namely the velocity field, the pressure in the pipe, the type of interaction between the fluid and the walls and the parameters for the inlet and the outlet. The remaining physical mechanic parameters were the same of those used in the previous study. In the heat transfer it was taken into account the radiation toward the ambient, the convection with the air around the pipe and the convection with the water inside the tube. This mechanics where imposed as boundary conditions of the solid domains. In order to obtain a variation in the temperature, a linear heat source was introduced in the model to substitute the missing plate with the heat source. Moreover, to see if the pipe is cooled, the temperature of the solid was fixed with an initial value higher than the temperature of the fluid.

Since in this new case of study there are present two different types of physical phenomena, heat transfer and laminar flow, the program can use a different kind of physical interaction to run the simulation. In this case, the added mechanics phenomenon is the non-isothermal flow, which considers the effects of the difference in temperature in the fluid. Thanks to these considerations, the simulation procedures can take into account, if requested by the user, the difference in density and the turbulence created by different temperatures in the fluid flow.

After the definition of the mesh grid and the choice of the type of study to be performed, time-dependent in this simulation, the program is run and the results are obtained.

The first result that we analyse is the temperature distribution shown in Figure 48 and in Figure 49, only in the water domain, to make more clear the smaller differences of temperature presented.

As expected, from Figure 48 it is clear that the water is colder than the pipe and from Figure 49, it is visible the change of temperature obtained in the water while it goes through the pipe. Even in the first seconds of the simulation, when the difference of temperature is smaller than 1K. However, analysing the distribution of the temperature after some second the picture is different as shown in the Figure 50 for all the domains and in Figure 51 for the water domain.

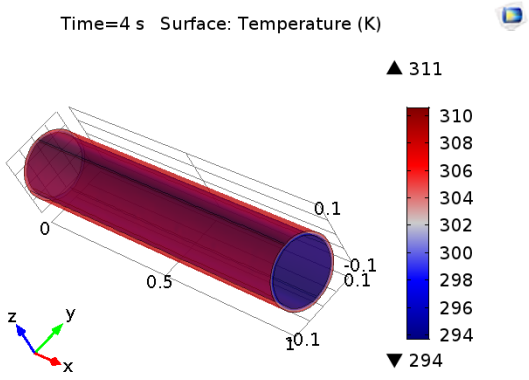

Figure 48 Temperature in a straight pipe after 4 s

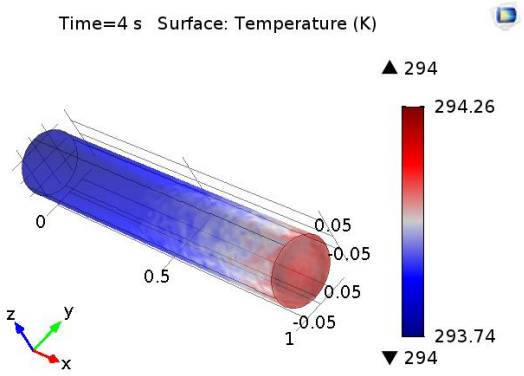

Figure 51 Temperature in the water passing through a straight pipe after 4 s

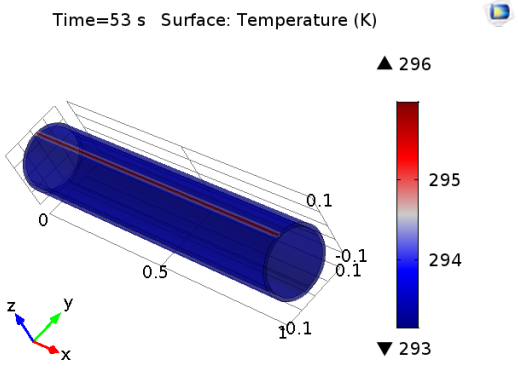

Figure 50 Temperature distribution in a straight pipe after 53 s

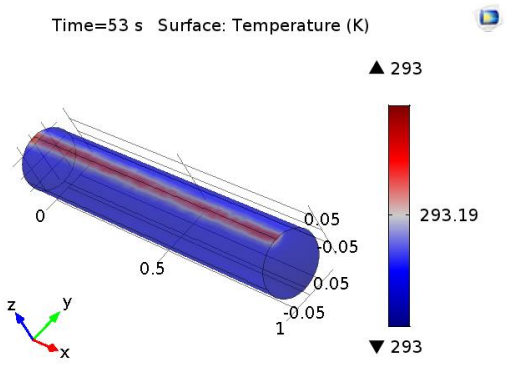

Figure 49 Temperature distribution in the water inside the pipe after 53 s

It clear from the images above that after some second the flowing water cools down the pipe apart from the line where the heat source is present that is some degrees hotter. In the water domain a similar change is seen with the passing of time, in fact in the first second the water is heated by the complete surface of the pipe and the temperature will be therefore higher in the last sections of the pipe more close to the outlet. On the other hand, after almost a minute that the water flows in the conduct the walls, as said before, will be almost completely cool down and the temperature of the water that is more far from the heat source is not affected by a change in temperature.

Another important result given by this simulation is the velocity field in the pipe. In fact, even if we give the velocity of the fluid as an input while defining the simulation, due to the interaction between the walls and the fluid and the time-dependent study the velocity field change during the time reaching an equilibrium determined by the pressure drop in the pipe. Moreover, where the fluid is in contact with the walls the fluid is not moving creating a gradient of velocity which has a peak in the centre and a minimum at the walls, as shown in Figure 52 and Figure 53 below.

The Figure 53 show how the maximum velocity increase in absolute value with the passing of time. Moreover, in the central area the speed of the fluid is more and more uniform and becomes more close to the maximum value, the red area is in facts growing with the passing of time.

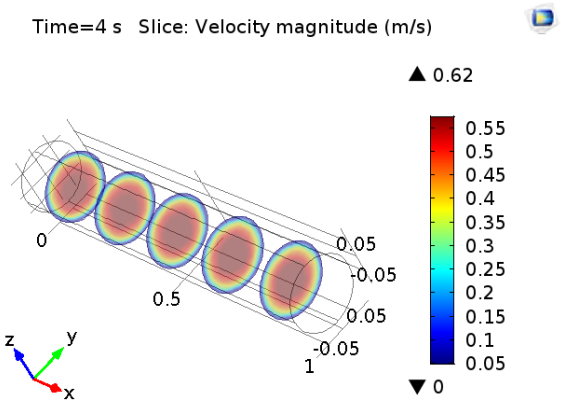

Figure 52 Velocity field after 4 s

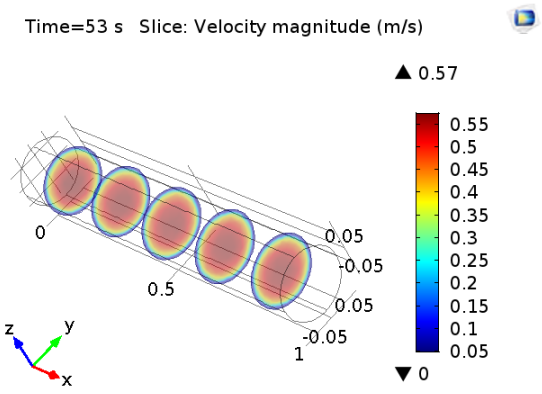

Figure 53 Velocity field after 53s

The last result that can be obtained from this simulation is pressure distribution in the pipe. The evolution of the pressure field in time is presented in the images below.

In Figure 54 is visible how the heat passing from the pipe to the water creates a higher pressure in the central part of the pipe. In the Figure 55 that follows is visible that the perturbation of the pressure due to the change in temperature is ended and the maximum values of pressure are at the end of the conduct.

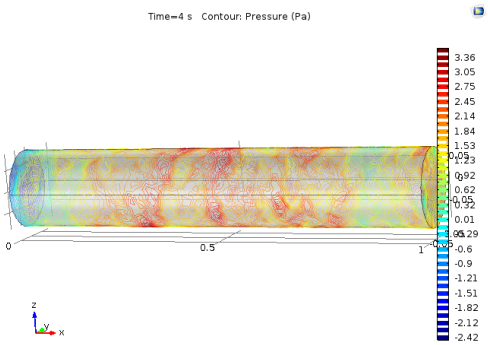

Figure 54 Pressure in the pipe after 4 s

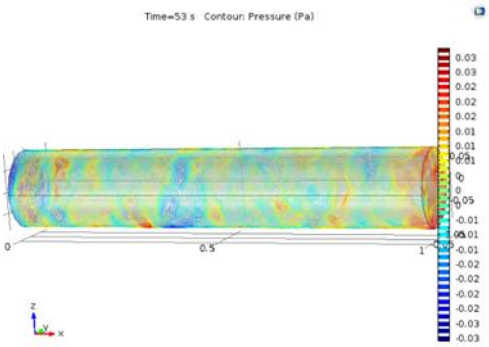

Figure 55 Pressure in the pipe after 53 s

A.3 Fluid flow in a twisted tube

After analysing the laminar fluid flow in a straight tube, the problem has been complicated introducing the fluid dynamics in a twisted tube that touches a plate in which is present a domain heat source. To study this case the new geometry has been created inside the software and four curves were introduced in the pipe. The new geometry is shown in Figure 56 below.

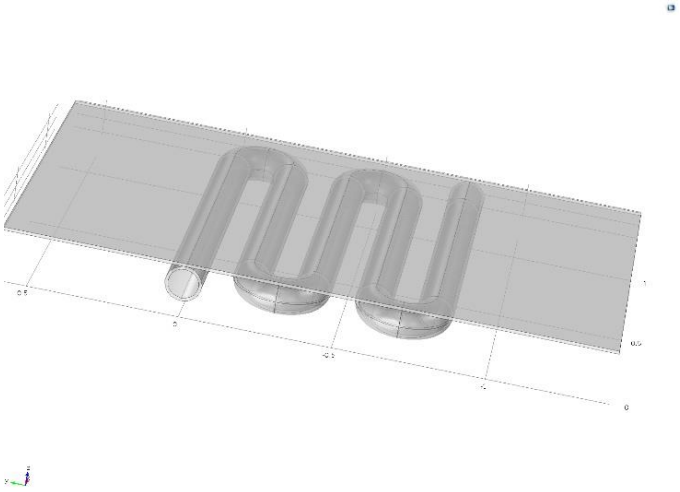

Figure 56 Geometry of the plate cooled by a twisted tube

The materials in this simulation were maintained equal to those used in the previous simulation and are: iron alloy 1030 (UNS G10300) and the water.

The physical properties used in this case of study were the heat transfer in fluid and solid and the laminar fluid flow. The heat transfer was divided into three different components the radiation with the external atmosphere and the two different convections, the one with the air that surrounds the geometry and the

one with the water flowing inside the pipe. The laminar flow was used to define the speed that the water has when it flows in the pipe.

The mesh introduced was more detailed than those used in the previous simulations and it was generated using a predefined method. The use of a more detailed mesh adds however an impact in the computation time of the simulation.

After the creation of the mesh the simulation was effectuated. Also in this simulation was decided to perform a time-dependent study defining a time of one hour with a time step of one minute. The temperature obtained is shown in the Figure 57 and in Figure 58 below. In particular in the first image is visible the temperature in the complete geometry while in the second picture is underlined the temperature in the water domain, otherwise not clear for scale reasons, both the images show the situation after 5 minutes that the water is flowing in the pipe.

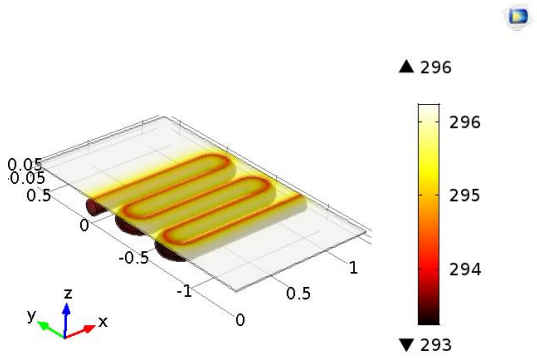

Figure 57 Temperature distribution in the geometry after 5 minutes

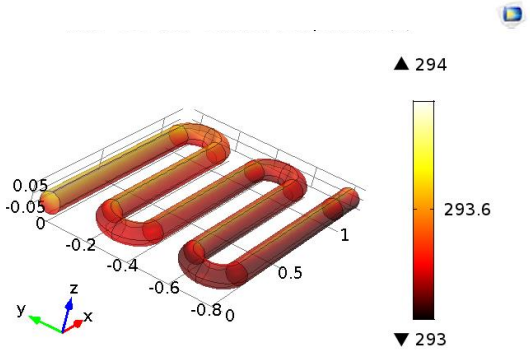

Figure 58 Temperature distribution in the fluid after 5 minutes

In the Figure 57 is observable how after 5 minutes the temperature in the plate is not very affected by the cooling water and the areas with a lower temperature are those in direct contact with the refrigerated pipe. Looking at the water temperature distribution, visible in Figure 58, is clear that the influence of the plate is more noticeable in the part of the fluid that flows closer to it and is clearly visible how the fluid gets hotter while flowing in the pipe.

After half an hour from the beginning of the simulation the results presented become more interesting, in fact the plate shows a central area where the temperature decreases and reaches a temperature more similar to the temperature of the pipe (Figure 59). On the fluid side after 30 minutes is visible how with the passing of time the temperature difference between the inlet and the outlet increases in value (Figure 60).

In the last frame of the simulation, after 60 minutes, the gradient of temperature distribution obtained after 30 minutes is even more defined. The difference of temperature in the plate is bigger and can be observed how the red area is increasing while in the water domain the colour distribution is very similar even if the scale is bigger and therefore the temperature difference is increasing.

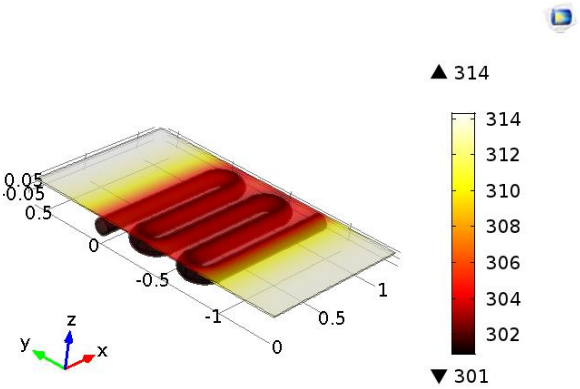

Figure 60 Temperature distribution of the geometry after 30 minutes

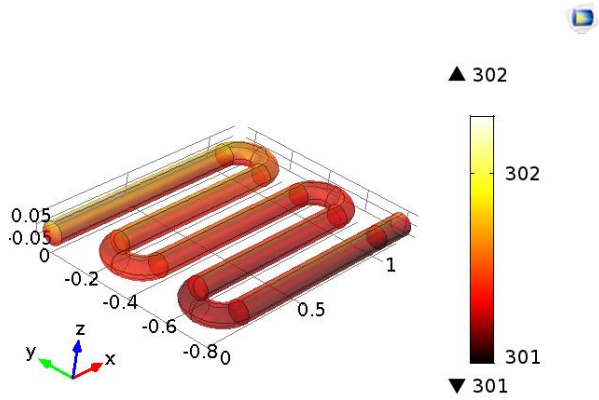

Figure 59 Temperature distribution of the fluid after 30 minutes

Analysing the distribution of water speed in the pipe can be seen how the velocity distribution changes at the beginning in the first minutes (Figure 63) but then it reaches a stable distribution of velocities and then the variation affects only the module of the speed. The two figures 64 and 65 show an almost identical distribution of colours and also from the scale is possible to understand that the speed of the water is not changing. This means that the temperature in the fluid has reached a point of equilibrium. Moreover in the pictures can be seen how the curves have an influence on the fluid speed crating areas where the speed drops close to the inner border of the curve.

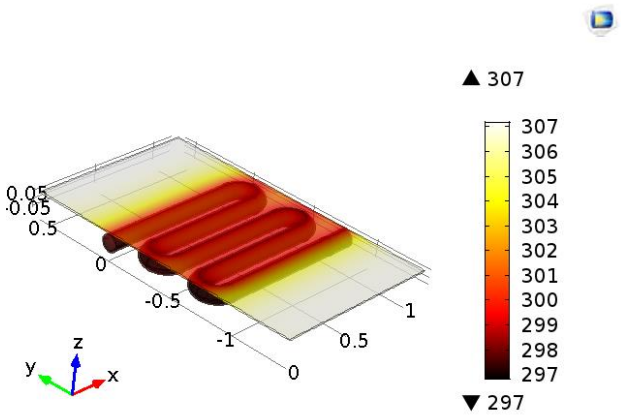

Figure 62 Temperature distribution in the geometry after 60 minutes

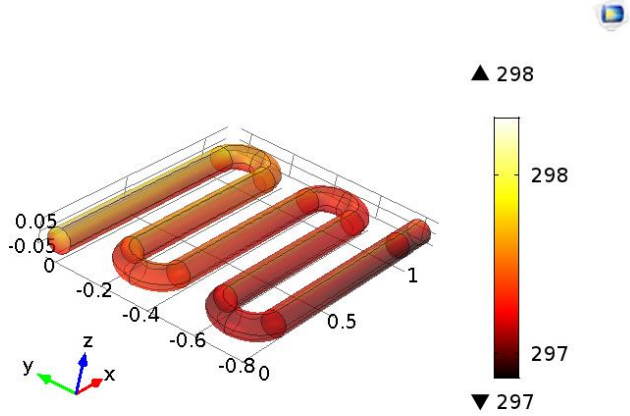

Figure 61 Temperature distribution in the fluid after 60 minutes

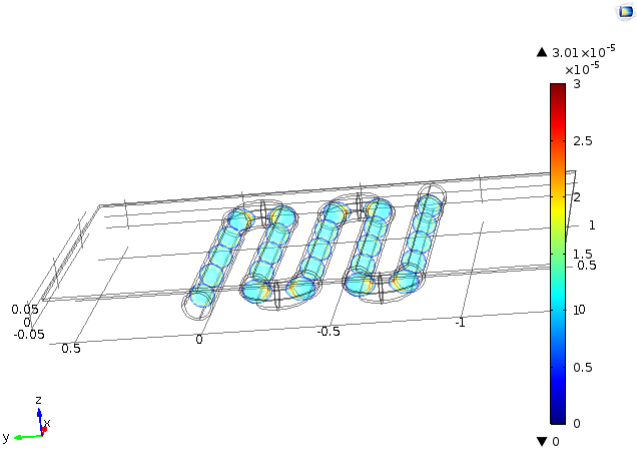

Figure 65 Velocity distribution in the twisted pipe at the beginning of the hour

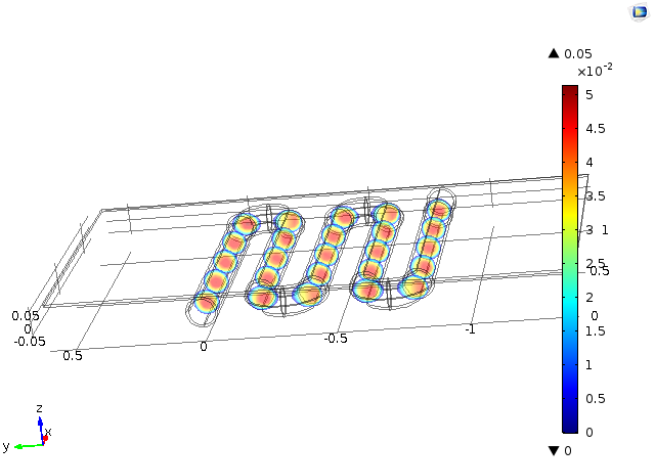

Figure 63 Velocity distribution in the twisted pipe after 20 minutes

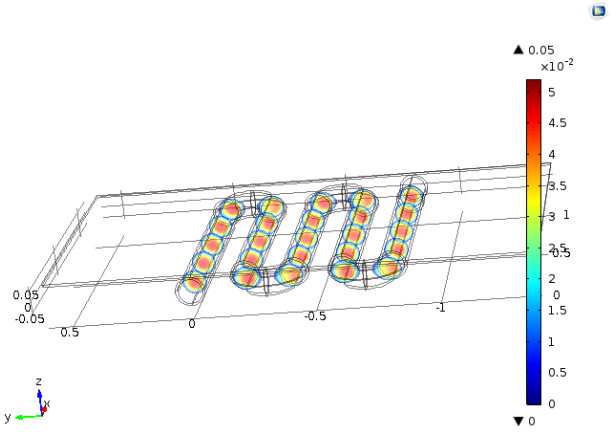

Figure 64 Velocity distribution in the twisted pipe after 1 hour